# CROSS TALK BETWEEN MACROPHAGES AND GLIOMA STEM CELLS

By

LEORA MOLLY NUSBLAT

A dissertation submitted to the

Graduate School – New Brunswick

and

The Graduate School of Biomedical Sciences

University of Medicine and Dentistry of New Jersey

In partial fulfillment of the requirements

For the degree of

Doctor of Philosophy

Graduate Program in Biomedical Engineering

Written under the direction of

Charles M. Roth, PhD

And approved by

_____

_____

_____

_____

New Brunswick, New Jersey

October 2014

**ABSTRACT OF THE DISSERTATION**

Cross Talk Between Macrophages and Glioma Stem Cells

By LEORA MOLLY NUSBLAT

Dissertation Director:

Charles M. Roth, PhD

Given its extremely poor prognosis, there is a pressing need for improved understanding of the biology of glioblastoma multiforme (GBM), including the roles of tumor subpopulations, such as macrophages, that contribute to tumor growth and therapeutic resistance. DNA alkylating agents, such as temozolomide and carmustine, are the current gold standard drug treatment for GBM, yet resistance occurs and is attributable to a subset of cancer stem cells (CSCs). The mechanisms by which the CSC state is produced and promotes drug resistance are not well understood, but molecular pathways are beginning to emerge. We investigated the interplay between CSCs and macrophages via co-culture. The results showed that macrophages communicate with and influence CSC functions via a paracrine loop. Specifically, the levels of an M2 macrophage-specific secreted cytokine, TGF-β1, were elevated in the presence of CSCs, but whether the cells were plated as contacting or non-contacting co-cultures did not affect the results. Furthermore, co-culturing with CSCs resulted in enhanced expression of M2 markers in macrophages that were previously polarized to the M1 phenotype. A major player in the cross talk is the inflammatory transcription factor, STAT3, produced by CSCs, which recruits and subsequently modulates macrophages to become immunosuppressive, maintaining CSC stemness. Another intriguing target is the transcription factor, HIF-2$\alpha$, the expression of which is markedly increased in hypoxic

CSCs. Here, we utilized short interfering RNA (siRNA) to silence CSC targets. For the delivery of siRNA cargo, cationic amphiphilic macromolecule (CAM) – lipid complexes were co-developed. We discovered that addition of certain levels of lipid induces pH-dependent instabilities that promote intracellular delivery and release from endosomes, leading to efficient gene silencing. We utilized these CAM-lipid complexes or Lipofectamine for silencing experiments. It was observed in both glioblastoma patient and cell line-derived CSCs that neurosphere formation, proliferation rate, chemoresistance, migration towards macrophage conditioned media, and matrix degradation were elevated compared to bulk tumor. Addition of STAT3 siRNA potentiated modestly the effects of carmustine on CSCs. HIF-2$\alpha$ siRNA had a significant effect on hypoxic CSC functions and induced their differentiation. Thus, disrupting CSC stemness or their cross talk with macrophages may be viable avenues for next-generation cancer therapeutics.

## DEDICATION

To my family with love

## ACKNOWLEDGEMENTS

I am extremely thankful for all the support that I have received throughout my studies at Rutgers. I am fortunate to have been advised by Dr. Charles Roth, who allowed me tremendous flexibility in my thesis focus and to partake in collaborative research projects. I thank him for being so generous with his time guiding me, ranging from experimental design and critical thinking to grant writing and technical presentations. I would also like to thank my committee members, Dr. Martin Yarmush, Dr. Li Cai, and Dr. John Glod, for advising me from the start. Your insightful comments on my research were truly appreciated.

I would like to extend my sincerest appreciation to our collaborator, Dr. Kathryn Uhrich, and her team for their helpful brainstorming discussions, enthusiasm, and synthesis expertise. I would especially like to thank Dr. Li Gu for working with me in tandem designing, preparing, and characterizing the micelle delivery system.

I am extremely grateful to our collaborator, Dr. Michael Masterman-Smith, for his generous gift of patient-derived glioblastoma stem cells. I thank him for reaching out to help, discussing experiments, new research ideas, and the intricacies of starting out in industry, and inspiring me to do great work.

I thank all the members, both past and present, of the Roth, Yarmush, and Berthiaume labs, for taking the time to provide technical advice on using the confocal microscope and sorting monocytes from blood samples. The students, faculty, and staff that I have worked with in BME, both for research pursuits and during my Teaching Assistantships, have been extremely helpful in their feedback and support.

Last, my family played a crucial role in my research successes. I am extremely grateful to my parents for their unconditional support over the years to pursue my interests. I thank my siblings and cousins for devoting their summers to do volunteer and other work experiences with me in research and medical facilities. My belated grandparents instilled in me the importance of hard work and I am so fortunate for them to have been such a huge part of my life. I am thankful for their encouragement to pursue a scientific career, listening to all my presentations and explanations about my research. Finally, I thank my fiancé, Matan, for his constant love and support through all the difficult moments and exciting achievements. Thank you for always being confident in me, teaching me to engage the audience, and for sacrificing personal time together. Thank you all for your support in helping me achieve this career milestone.

## TABLE OF CONTENTS

## LIST OF ILLUSTRATIONS

# 1 CHAPTER 1: INTRODUCTION

## 1.1 CSCS IN GBM

Glioblastoma multiforme (GBM) carries a terrible prognosis of merely 15 months[1] even following aggressive treatment with surgery, radiation and chemotherapy. Some of the factors involved in resistance could be attributed to the interaction with other cell types in the tumor milieu. There is a growing appreciation of the fact that GBM cannot be considered in the paradigm of a single malignancy. Rather, it is a heterogeneous disease with multiple cell subpopulations interacting in a dynamic manner. The persistent recurrence of brain tumors after chemotherapy has been speculated to be due to the presence of cancer stem cells (CSCs)[2]. These cells have a capacity for efficient DNA repair, self-renewal, multipotency, and recapitulation of tumors *in vivo*. Even though these cells constitute only a small fraction of cells in a tumor, they are able to self-renew, promote regrowth and metastases, and infiltrate normal brain tissues[3], making their eradication difficult. They were first isolated in acute myeloid leukemia, and identified in many other types of cancer including gliomas, which were discovered by both Singh and Galli's groups[1]. Their identification in multiple tumors makes them an ideal target in drug development. The stemness of the CSCs is maintained by an incompletely understood confluence of physiological and cell-mediated factors within the tumor microenvironment, including pH, hypoxia and levels of soluble factors secreted by neighboring cells[4-6]. In turn, CSCs actively maintain the microenvironment[7].

## 1.2 MACROPHAGES IN GBM

The GBM microenvironment contains not only malignant cells, but also several other cell types including tumor associated macrophages. In the context of tumors, macrophages

home to regions of hypoxia and their presence is associated with a high mortality rate[8,9]. Macrophages provide a number of signals to tumor cells[10,11], but their exact role in tumor response is still emerging. Although macrophages play an immunostimulatory role in classical macrophage polarization (M1), during wound healing and infection response, when recruited to tumors, they have been correlated with metastasis. This is due to alternative macrophage polarization (M2), resulting in immunosuppression, extracellular matrix remodeling, and tumor growth and metastasis[12-14]. In fact, the presence of macrophages in tumors is associated with a high mortality rate. Microglial cells have been shown to contribute up to 30% of a brain tumor mass and play a role in glioblastoma cell invasion[10]. Additionally, it has been shown that M2 macrophages attract vessel-associated stem cells and utilize matrix metalloproteinase, MMP-9 in regulating cell migration, thus indicating that M2 macrophages are involved in matrix remodeling[15]. They also contribute to tumor angiogenesis via VEGF[16,17].

## 1.3 SIGNALING BETWEEN CSCS AND MACROPHAGES

The signaling among cells in the tumor microenvironment plays an important role in tumor growth and resistance. The mechanisms by which monocyte-derived cells are recruited to tumors and reprogrammed have yet to be fully established due to their heterogeneity and differential functions. Macrophages within GBM are comprised of microglia, which reside in the brain and continuously survey the intraneuronal space, and tumor-associated macrophages, which are transported to the brain via the bloodstream and can be found in the outer boundaries of the brain[18].

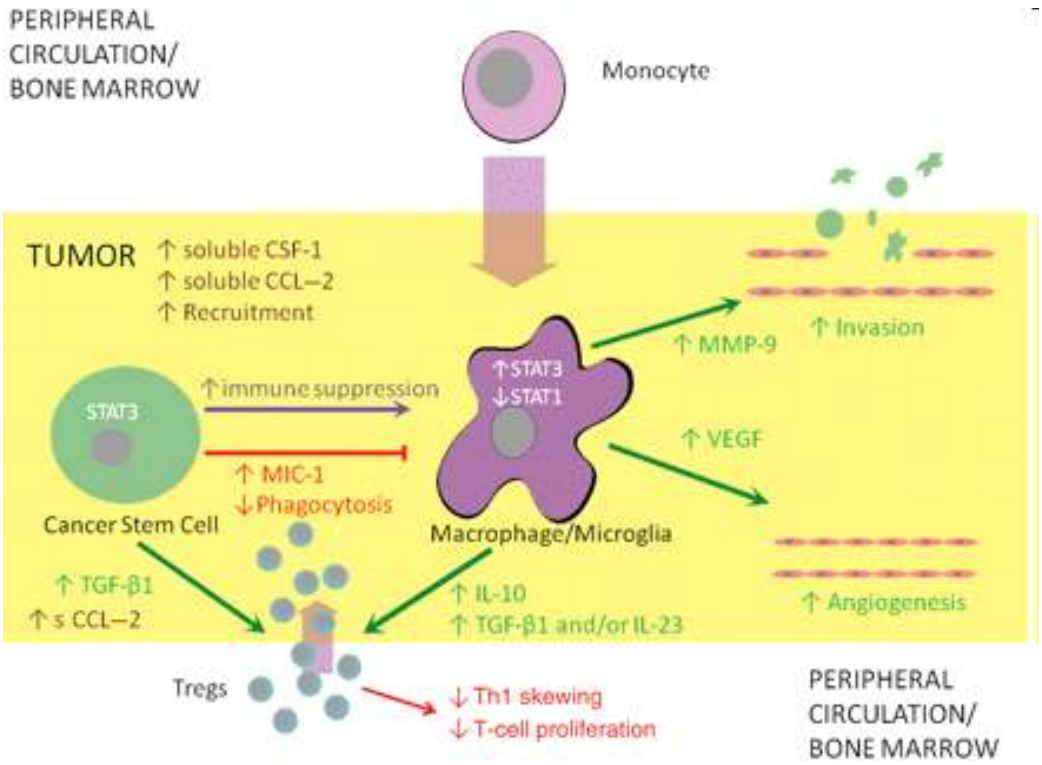


**Figure 1. CSCs promote M2 macrophage activation (adapted)[19]**

**CSCs recruit monocytes and mediate their differentiation into M2 macrophages, which have reduced phagocytosis, produce immunosuppressive cytokines, and contribute to invasion and angiogenesis. The immunosuppressive functions of CSCs are mediated by STAT3.**

The interplay between cancer stem cells and macrophages has been demonstrated[20,21], with evidence pointing to a role for the signal transducer and activator of transcription 3 (STAT3) pathway, a transcription factor in the IL-6 pathway. IL-6 is produced by non-stem glioma cells, as well as by endothelial and immune cells, and IL-6 receptors, gp130 and IL-6Rα, are expressed on glioma stem cells[22-24]. The expression of IL-6 is stimulated by hypoxia[25]. It has been shown that STAT3, expressed by CSCs, is involved in monocyte recruitment and subsequent M2 macrophage polarization, as

illustrated in Figure 1[19]. Additionally, TGF-β1, produced by CSCs via STAT3 signaling, regulates immune responses of macrophages[26]. STAT3 is a potential target for therapy as its silencing suppresses GBM cell growth and has been shown to enhance the effects of chemotherapeutics and radiotherapies[27,28]. When p-STAT3 is blocked in CSCs, proliferation and neurosphere formation are impaired and CSC-mediated immunosuppression is blocked. Thus, CSCs contribute to macrophage polarization in a manner that involves STAT3. While the reciprocal effect of macrophages on the CSC phenotype is less well established, the propensity of macrophages to utilize inflammatory pathways such as IL-6/STAT3 suggests that such an effect is quite plausible.

Following their recruitment and polarization, microglia promote invasion by secreting proMMP2, an inactive form of the MMP, which is then activated by secreted factors from glioblastoma cells[29]. Microglia is a primary source of interleukin 1β (IL-1β), which can enhance expression of TGF-β, leading to an anti-inflammatory response marked by lymphocyte proliferation, reduced immune cell activation, and inhibition of antigen presentation[26]. Also, TGF-β can lead to angiogenesis (via VEGF), proliferation (via EGFR), and invasion (via MMP-9). Glioma cells also secrete EGF, enhancing microglial motility[30]. Additionally, it has been shown that M2 macrophages attract vessel-associated stem cells and utilize matrix metalloproteinase, MMP-9 in regulating cell migration[15]. This work suggests that M2 macrophages are involved in matrix remodeling due to their secretion of MMPs. However, whether M2 macrophages attract CSCs has not been established. Also, these studies have not focused on the motility and invasiveness of CSCs specifically in the presence of macrophages.

.

## 1.4 DESIGNING SIRNA DELIVERY VEHICLES FOR IMPROVED GENE SILENCING

Short interfering RNA (siRNA) is a powerful tool for sequence-specific silencing of target genes in drug discovery and therapeutically. It consists of 19-23 nucleotides and acts on complementary mRNA sequences, utilizing the RNA-induced silencing complex (RISC) for their degradation[31]. This approach of silencing endogenous genes has been demonstrated in CSCs[32] using an siRNA for Notch-1, resulting in decreased CSC proliferation and reduced tumor growth. However, unmodified siRNA is taken up poorly into cells and degraded by serum proteins.

Approaches in designing an effective siRNA delivery system include ensuring that they target the region of interest (tumors), are protected from degradation by serum proteases in blood, limit excretion through kidneys, minimize dosage due to “off-target” effects, and are shielded from the immune system[33]. Encapsulating siRNA within liposomes and modifying them with functional groups is a useful approach. Liposomes have been used as a nonviral delivery vehicle for cancer drugs. In particular, cationic liposomes have been shown to target tumors due to their leaky vasculature, allowing them to enter tumors through the gaps[34]. Cationic polymer-based and lipid-based systems[35,36], cell-penetrating peptides[37,38], and chemically modified siRNAs[39] have been developed as vehicles to deliver siRNA[40]. Liposomes can complex with siRNA electrostatically. Attaching PEG to liposomes creates sterically stabilized or ‘stealth’ liposomes that increase circulation time in blood by shielding them from serum proteins and macrophage engulfment. However, better non-viral siRNA delivery systems are still needed with improved efficiency and minimal cytotoxicity in order for them to be useful clinically.

## 1.5 TARGETING THE CSC MICROENVIRONMENT

Like most solid tumors, GBM tumors contain regions of hypoxia due to avascular regions, which help maintain stem cells in tumors, in part by preventing the differentiation of stem cells. These regions of hypoxia are particularly apparent in gliomas and cause oxygen levels to drop below physiological levels (1-7%)[41]. Disrupting these hypoxic regions may provide a route to stem cell targeting[42]. Instead of targeting the hypoxic niche itself, a challenging feat, a better approach may be to target the signaling response to hypoxic conditions, mediated through hypoxia inducible factors (HIFs). HIFs are heterodimers with an alpha and beta subunit and function as transcription factors. Under normoxic conditions, HIF is complexed to pVHL, resulting in its ubiquitization and degradation in the proteosome. In the presence of hypoxia, VHL dissociates from HIF, causing it be stabilized and translocated to the nucleus where it dimerizes with HIF$\beta$ and transcribes hypoxia proteins.

Hypoxic conditions are an important factor in a tumor model since it is reflective of the tumor microenvironment where CSCs are enriched. Under hypoxic conditions, HIFs are upregulated. Both HIF-1 and HIF-2 isoforms are expressed in gliomas and their roles seem to be overlapping. Both HIF-1 and HIF-2 alpha and beta complexes bind hypoxia-response elements (HREs) in the promoters of many genes, such as VEGF, in order to upregulate them in response to hypoxia. However, while HIF-1$\alpha$ and HIF-2$\alpha$ are 75% homologous, they have several notable differences. Glioma CSCs overexpress HIF-2$\alpha$ in as high as 5% $O_2$ levels, while HIF-1$\alpha$ is elevated only when the concentration is <1%[5]. HIF-2$\alpha$ is an attractive target since hypoxia induces HIF-2$\alpha$ exclusively in CSCs, while HIF-1$\alpha$ is induced in both CSCs and non-stem tumor cells[5]. Yet, surprisingly, HIF-

2α expression has not been detected in normal human macrophages or in non-stem tumor cells. Some groups have reported the immunosuppressive role of HIF-2α in TAMs[43]. Although both HIF-1α and HIF-2α are expressed in macrophages, HIF-2α accumulation in TAMs is correlated with high tumor vascularity and tumor grade in many cancers including glioblastoma[9].

## 1.6 DISSERTATION SUMMARY

The long-term goal of this work is to improve treatment strategies for eradicating CSCs in GBM. To date, advancements have been limited due to the resistant CSC population that remains following treatment. Therefore, better targets need to be identified. Here, we explore the effects of silencing two potential CSC targets with complementary putative mechanisms. First, we investigate the effects of silencing HIF-2α, because of its specificity for the hypoxic CSC environment. Second, we investigate the effects of silencing STAT3, which appears to have a role in mediating the CSC-macrophage cross-talk. Ultimately, we envision a combination approach to CSC therapy that disrupts the maintenance of the stem-like state by jamming the cross talk with other cell types along with an agent that selectively cripples the CSC cells directly. SiRNA provides the means to perform target validation in the near-term and may prove a viable therapeutic approach in the long-term.

In Chapter 2, we identified that a paracrine loop is involved in the cross talk between CSCs and macrophages. Previous reports implicated that macrophages are involved in juxtacrine signaling with tumor cells by the enhanced activation of STAT3 in cells directly

co-cultured[44], but these studies focused on the bulk glioma tumor cells and not enriched stem cells. Here, we demonstrated that indirectly separated co-cultures of CSCs influence macrophage polarization to the M2 phenotype, as measured by ELISA for TGF-β1. Additionally, we characterized the CSCs and confirmed their stemness by neurosphere formation, proliferation, and immunofluorescence of neural stem cell markers. In an effort to target the CSC population or disrupt the cross talk with macrophages, silencing experiments were performed. We observed inhibition of STAT3 reduced the growth of tumor cells and other CSC functions, consistent with results reported for bulk glioma cells.

In Chapter 3, we co-developed cationic amphiphilic macromolecule (CAM) – lipid complexes for gene silencing. By varying lipids added to the previously designed CAM micellar system, we were able to efficiently deliver siRNA to GBM cells. Additionally, this system was pH-sensitive, leading to its efficient uptake and endosomal release.

In Chapter 4, we tested the delivery vehicle and also used Lipofectamine for transfection experiments in CSCs. The chemotherapeutic resistance and migratory capacity to macrophage conditioned media had an additive effect when STAT3 or HIF-2α were silenced, but the effects were more pronounced for HIF-2α, which is exclusively overexpressed in hypoxic CSCs.

# 2 CHAPTER 2: UNDERSTANDING THE CROSS TALK BETWEEN MACROPHAGES AND CSCS

Note: This chapter is partially reproduced from sections of the following publication:

L.M. Nusblat, M. Carroll, and C.M. Roth. Cross talk between M2 macrophages and glioma stem cells (*To be submitted 09/2014)*

## 2.1 INTRODUCTION

CSCs are important in macrophage polarization, but the reciprocal effect of macrophages on the CSC phenotype is unclear. We hypothesized that macrophages can enhance CSC proliferation, neurosphere formation, chemotherapeutic resistance, migration, ECM degradation, and cytokine secretion. In this chapter, we demonstrate that M2 macrophages derived from peripheral blood monocytes enhance CSC functions, and that this occurs via TGF-β1 signaling. Furthermore, we show that siRNA-mediated silencing of STAT3 reduces the chemoresponsiveness and migratory abilities of the CSCs.

## 2.2 METHODS

### 2.2.1 CSC DERIVATION AND CHARACTERIZATION

The CSCs were derived as described in the literature[45]. Briefly, serial dilutions were made of U87 cells in neural stem cell (NSC) media containing DMEM/F12 1:1 media, B27 serum-free supplement (1×), penicillin (10,000 IU/mL), streptomycin (10,000 µg/mL), 20 ng/mL rhFGF (Invitrogen), 50 ng/mL rhEGF (Invitrogen), HEPES 1 M

solution, and 5 ug/mL heparin (Sigma-Aldrich). Dilutions were continued until neurospheres formed. CSCs were characterized based on their pluripotency, limiting dilution assays, and immunofluorescence, which is consistent with other groups in the literature[46]. Using limiting dilution, neurospheres formed, which were capable of being passaged at least 10 times. The neurosphere formation rate was quantified, as well as their proliferative capacity. After primary spheres formed, they were dissociated and characterized. Supernatants were stored at -20°C for use as a conditioned medium and ELISA assays.

Primary samples obtained from patient brain tumors were obtained on Institutional review board-approved protocols (UCLA) and graded according to World Health Organization-approved guidelines. Stem cell enriched fractions from these samples were a generous gift from Dr. Masterman-Smith. Briefly, brain tumor tissues were isolated as described[47] and enriched for stem cells using serial dilutions in NSC media using the aforementioned protocol, forming brain tumor stem cells (BTSCs). Cells were seeded in a CSC growth and enrichment medium consisting of DMEM/F12 medium supplemented with 1:50 B27 (Invitrogen), 20 ng/ml bFGF (Invitrogen), 50 ng/mL EGF (Invitrogen), 1:100 penicillin/streptomycin (Invitrogen), 1:100 Glutamax (Invitrogen) and 5 ug/ml heparin (Sigma-Aldrich). Heparin, bFGF and EGF were supplemented weekly and Glutamax bi-weekly. Spheres were passaged using enzymatic dissociation with TrypLE and glass pipet dissociation[48].

### 2.2.2 DIFFERENTIATION OF MONOCYTE-DERIVED MACROPHAGES

Human peripheral blood mononuclear cells (PBMCs) were collected from healthy donor blood (Blood Center of New Jersey) that was de-identified and subsequently sorted by

density gradient centrifugation using Ficoll-Hypaque density gradient (Sigma-Aldrich). Further purification was performed using CD14 microbeads (Miltenyi Biotec) as specified by the manufacturer. Monocytes were cultured for 7-10 days in RPMI 1640 supplemented with 10% FBS, 1% P/S, 4mM L-glutamine, and 50 U/mL GM-CSF (R&D Systems). Following differentiation, cells were primed with either 1 μg/mL LPS or IL-4 (Sigma-Aldrich) for 2 days, resulting in M1 or M2 macrophages, respectively.

### 2.2.3 CHEMOTHERAPEUTIC EFFECT OF STAT3 SIRNA

An siRNA sequence (5'-AAC AUC UGC CUA GAU CGG CUA dTdT-3'; 3'-dTdT GUA GAC GGA UCU AGC CGA U-5') targeted against human STAT3 (Dharmacon) was delivered to cells using Lipofectamine 2000 as described by the manufacturer (Invitrogen). Silencer Select Negative Control siRNA (Invitrogen) was used as a control, non-targeting sequence. After 24 h, carmustine was added to the media. After 48 h, an MTT assay (Promega) was performed to evaluate viability as a measure of chemotherapeutic response to a combined STAT3 siRNA and carmustine therapy.

### 2.2.4 EXTRACELLULAR MATRIX DEGRADATION

CSCs were plated on a DQ-collagen IV (Invitrogen) thin film overnight. Since the matrix is fluorescently labeled, degraded areas were indicated by the presence of fluorescence within the cells. Fluorescent areas, indicating areas of degradation, were quantified in Image J and normalized to total cell area.

### 2.2.5 MIGRATION ASSAY

Transwell filter chambers with 8 µm pores (BD Biosciences) were used in a 24-well plate for the migration assay. U87, CSCs, or BTSCs (700,000 cells/350 µl) within DMEM/F12 medium were seeded into the upper well of the insert, while the lower well contained 600 µl of LPS or IL-4 stimulated macrophage conditioned media, LPS or IL-4 supplemented macrophage media, or unconditioned macrophage media (RPMI, 10% FBS, 1% P/S, and 4mM L-glutamine). Chambers were incubated at 37 °C and the cells were allowed to migrate for 24 h. The outer side of the insert was gently rinsed with PBS prior to imaging. Migrated cells were counted under a light microscope in 10 randomly chosen fields in the bottom well with 10× objective. At least 50 cells were analyzed per experiment. All other co-culture experiments were done using 4 µm pore size transwell chambers (BD Biosciences).

### 2.2.6 ELISA MEASUREMENT OF CYTOKINES IN MEDIUM CONDITIONED BY CSCS

The supernatants of CSCs cultured for 7 days were collected and stored at -20°C, and concentrations of cytokine were measured by a TGF-β1 ELISA assay (Invitrogen). The optical density was measured at 450 nm using a plate reader. The detection limit for TGF-β1 was 31 pg/mL as indicated in the manufacturer's protocol.

### 2.2.7 STATISTICS

The data is presented as means ± standard error of the mean (SEM). Each experiment was repeated three times unless otherwise noted and comparisons were done using one-way ANOVA and post-hoc analysis, as indicated in the figure legends.

## 2.3 RESULTS AND DISCUSSION

It has been demonstrated previously that CSCs could be isolated from primary brain tumor specimens[2] or from glioma cell lines[49,50]. Here, CSCs were successfully isolated from a GBM cell line, U87, or from patient specimens, BTSC, through incubation in gradually increasing proportions of NSC media for 10 days[45,46,51]. Resulting neurospheres expressed the stem cell markers, nestin and CD133, as confirmed by immunofluorescence and discussed in chapter 4. To further confirm the presence of CSCs, neurosphere and proliferation assays were performed.

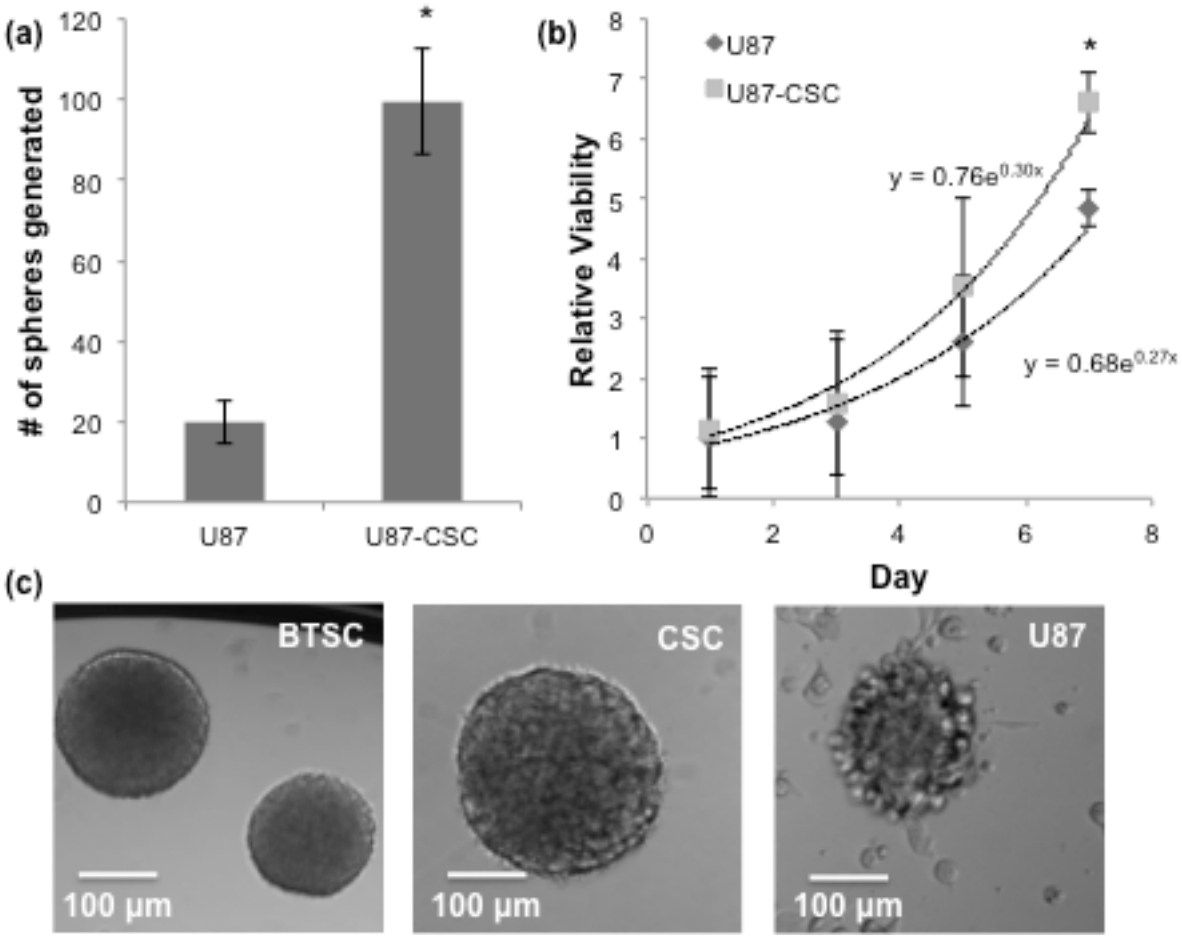


**Figure 2. Characterization of CSCs isolated from U87 cells**

**Monolayers of U87 and CSCs were plated at 1,000 cells/well of a 96-well plate. (a) Neurospheres generated after 7 days incubation in NSC medium were counted within each well. (b) Relative viability during 7 days of growth was measured by**

**MTS assay and resulting neurospheres are shown in (c); $p<0.05$, N=3.**

Seven days after plating single cells in NSC medium, CSCs formed 5 times as many self-aggregating neurospheres as did U87s (Figure 2a). To quantify cell proliferation on dissociated spheres after day 7, an MTS assay was performed. CSC viability increased at a slightly faster rate than U87s (Figure 2b). These results of faster neurosphere formation[48,52] and proliferation capacities[2] were also observed in BTSCs. Unlike for U87 cells, which formed both non-adherent spheres and adherent monolayers, CSCs or BTSCs formed only non-adherent spheres (Figure 2c). This suggests that "stem-like" cells were enriched.

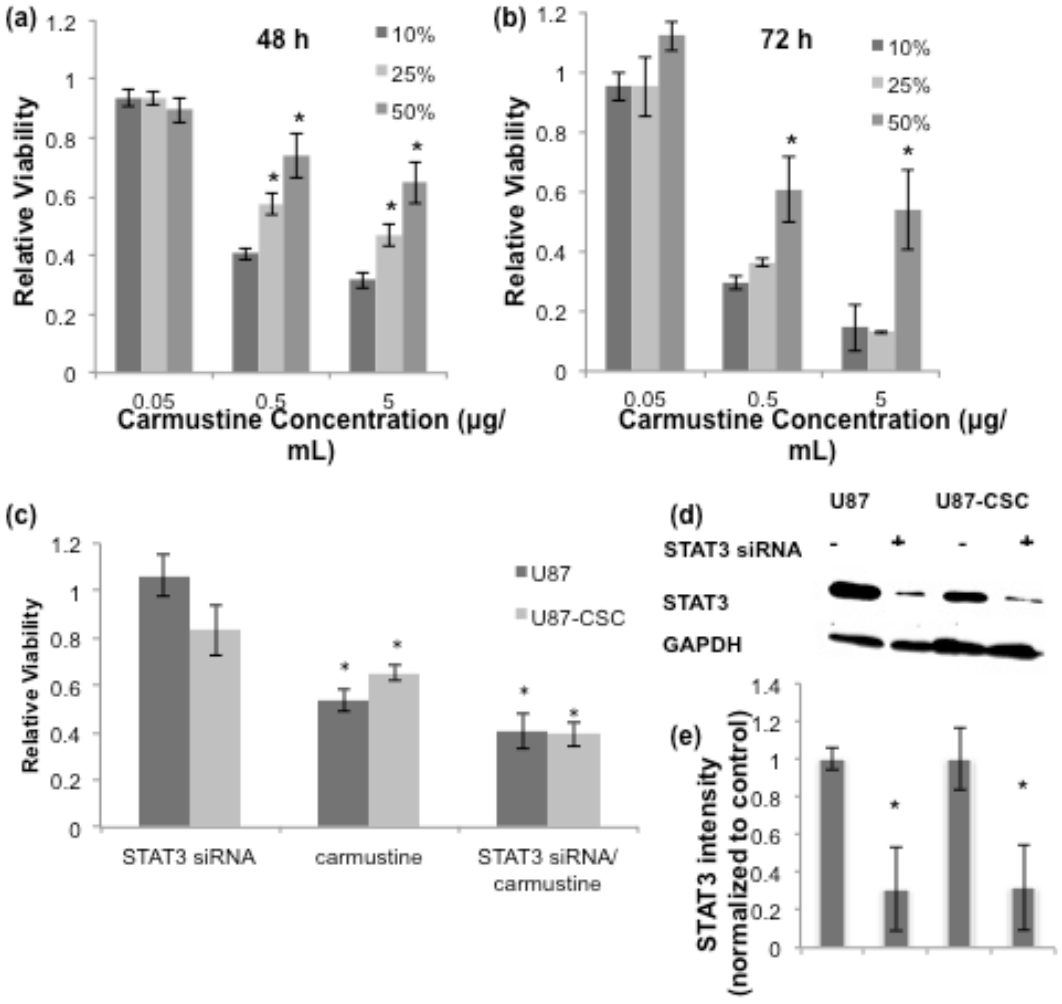


**Figure 3. CSCs are more responsive to carmustine and/or STAT3 siRNA treatment**

**The viability of co-cultured monolayers of U87s with 10%, 25%, and 50% CSCs was assessed via MTS assay at a) 48 h and b) 72 h following carmustine treatment; $p<0.05$. (c) CSC dissociated neurospheres were transfected with STAT3 siRNA or a non-targeting control siRNA for 6 h and subsequently treated with carmustine or a DMSO control for 48 h. Viability was measured by MTS assay. The absorbance at 450 nm was measured and normalized to a non-targeting sequence and subsequent DMSO control; * $p<0.05$, N=3. The carmustine**

**concentration used was 1000 µg/ml, chosen based on the $IC_{50}$. (d) Western blot of STAT3 siRNA silenced cells is shown. (e) Bar graphs are shown obtained by densitometric analysis of western blot data. Results (mean±S.E.M.) represent the ratio between STAT3 and GAPDH levels, and are normalized to a non-targeting siRNA control; $p<0.05$, N=3.**

CSCs are generally more resistant to drug treatment than bulk tumor cells. To test their chemotherapeutic response, CSCs and U87s were co-cultured as a monolayer and viability was assessed 48 and 72 h following carmustine treatment via MTS. In co-cultures of varying amounts of CSCs (10%, 25%, 50%), the relative viability after carmustine treatment was higher when more CSCs were present, as shown in Figure 3. This suggests that CSCs are more resistant to carmustine since increased CSC concentration reduces the therapeutic effect. Similar trends were observed with spheroid co-cultures grown using the hanging drop method (data not shown).

As STAT3 has recently emerged as a drug target for glioma and other cancers[28], we hypothesized that a combined carmustine and STAT3 siRNA therapy would be effective. Indeed, the viability of CSCs in the combined therapy was significantly reduced over carmustine alone, suggesting that STAT3 is involved in maintaining CSC resistance (Figure 3c). STAT3 silencing did not affect the viability of these cells. The maximum effect of siRNA was observed at 48 h and abated by 96 h (data not shown). The silencing achieved at 48 h was quantified in ImageJ was ~70% for both U87s and CSCs (Figure 3d and 3e). While STAT3 silencing enhanced the response to carmustine, the magnitude was less than expected based on the role of STAT3 *in vivo*[27,28]. To determine how STAT3 affects the role of macrophages on CSC function, monocytes were isolated from PMBCs, the myeloid precursors to normal and tumor-infiltrating

macrophages. They were then differentiated into macrophages and primed with either LPS or IL-4. This resulted in the formation of M1 and M2 macrophages from myeloid precursor cells, respectively. It was also observed that STAT3 silencing resulted in reduced migration towards macrophage conditioned media in both U87 and CSCs. This suggests that STAT3 could be mediating interactions among malignant tumor cells and other cells in the tumor milieu, specifically tumor activated macrophages.

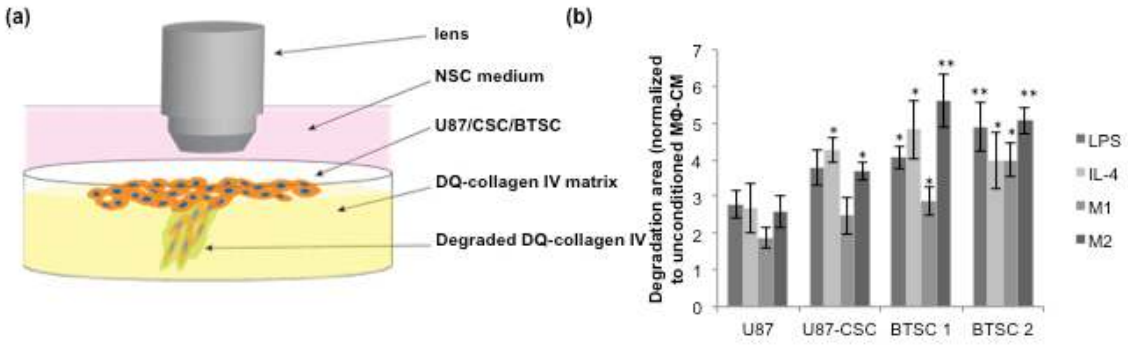


**Figure 4. Macrophages enhance collagen IV degradation of CSCs and BTSCs**

**(a) Schematic of the degradation assay is depicted of U87s, CSCs, or BTSCs plated on a DQ-collagen IV thin film and co-cultured in M2 macrophage conditioned media. (b) Fluorescent areas (degraded areas) were quantified in Image J and normalized to total cell area. Statistics compare the respective conditions to U87 cells; *p<0.05, **p<0.01, N=3.**

To further characterize the effect of M2 macrophages on CSC functions, a degradation assay was performed a degradation assay was performed of these cells plated on a DQ-collagen IV thin film overnight in the presence or absence of M2 conditioned media. The study was expanded to not only focus on CSC derived from a cell line, but also included two BTSCs. The degradation of extracellular matrix by CSCs on a DQ-collagen IV matrix was significantly increased over U87 cells when were co-cultured with M2

macrophages (Mϕ) (Figure 4). For BTSCs, this enhancement was even more pronounced. However, no significant differences in degradation were observed between slow proliferating (BTSC 2) and fast proliferating (BTSC 1) cell lines. Interestingly, the CSC or BTSC fractions exhibited increased degradation over U87 cells alone in both the presence and absence of macrophages, suggesting a pivotal role for CSCs in extracellular matrix (ECM) reorganization activities. This may be due to the upregulation of proteolytic enzymes involved in ECM remodeling.

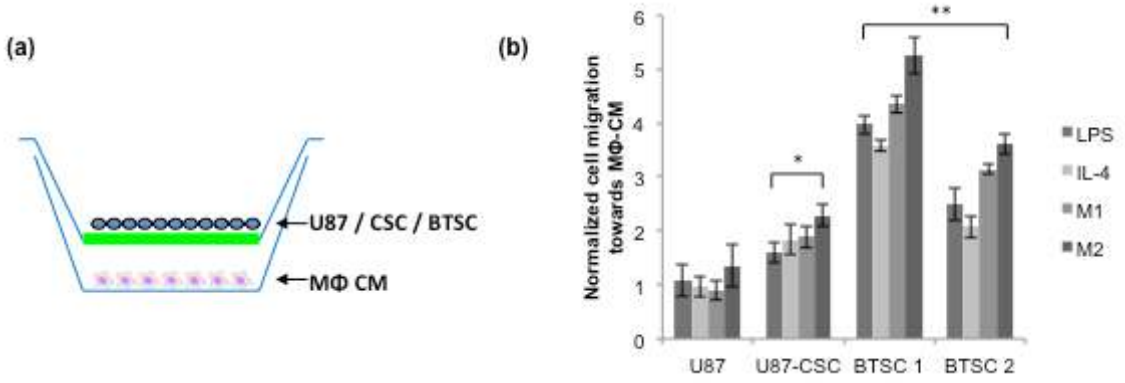


**Figure 5. Macrophages enhance CSC and BTSC migration**

**(a) A schematic of migration assay through a transwell system is illustrated. (b) The graph shows fold increase of cell migration over the non-conditioned medium treated cells. At least 50 cells per field and 10 fields were counted (10X) of cells that migrated through the transwell. Statistics compare the respective conditions to U87 cells; *p<0.05, **p<0.01, N=3.**

Using conditioned macrophage media, the migration of CSCs and U87s through an 8μm pore size membrane transwell was compared. Results showed that CSCs had increased migration towards macrophage conditioned media or their secreted factors compared to neural stem cell media, as shown in Figure 5. CSCs exhibited an increase

in migration to conditioned media from M1 or M2 macrophages or their secreted factors, LPS and IL-4, respectively. However, U87 migration was unchanged from control non-conditioned macrophage media. The migration was even further enhanced for BTSCs. Overall, the migration towards M2 conditioned media was increased over M1. Additionally, the values were slightly elevated for the M1 or M2 macrophage conditions, suggesting that LPS and IL-4 do not contribute entirely to the migration of CSCs and BTSCs. This suggests that macrophage secretions cause CSCs to move towards them. It has been previously demonstrated that secretions of CSCs derived from GBM cell lines recruit macrophages towards them[19], suggesting a paracrine loop.

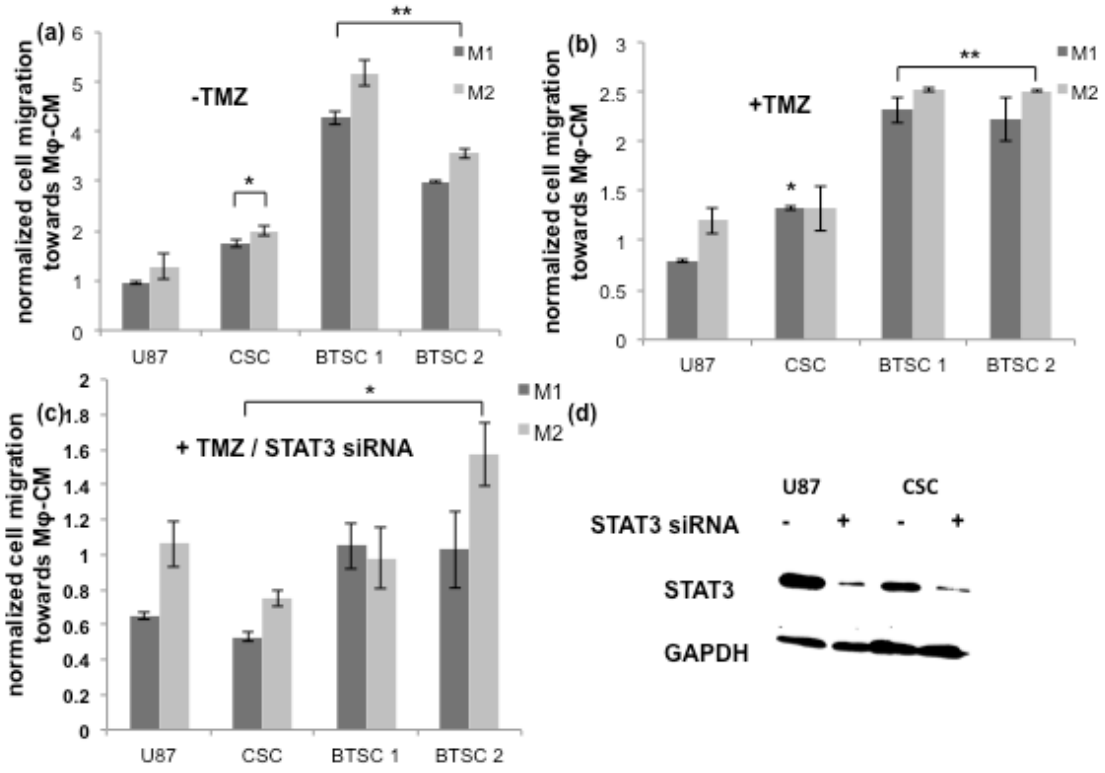


**Figure 6. Migration towards macrophage conditioned media is reduced in STAT3 silenced CSCs.**

**The TMZ concentration used was 1μM, chosen based on the $IC_{50}$ for dissociated neurospheres of either CSCs or BTSCs. Migration assays of U87s, CSCs, or BTSCs toward macrophage conditioned media were performed in cell monolayers that were (a) untreated or treated with (b) TMZ alone or (c) STAT3 siRNA and TMZ. Data was normalized to non-targeting control siRNA treated cells; *p<0.05, **p<0.01, N=3. (d) A western blot of STAT3 siRNA treated cells is shown. A non-targeting siRNA was used as a control.**

Since M2 macrophages have been associated with tumorogenicity, we next proposed to observe how their presence affects CSC functions. CSCs are strongly induced to migrate towards macrophage conditioned media. This effect was more pronounced for M2 compared to M1 conditioned media, as shown in Figure 6. Here, we investigated the response of another DNA alkylating agent, temozolomide (TMZ). In U87 or CSCs treated with TMZ, migratory affects were attenuated (Figure 6b). The combination treatment of TMZ and STAT3 siRNA further decreased migratory capacity, but this effect was not significant (Figure 6c). For future studies, we are interested in selectively eradicating CSCs, and doing this may require other drug targets.

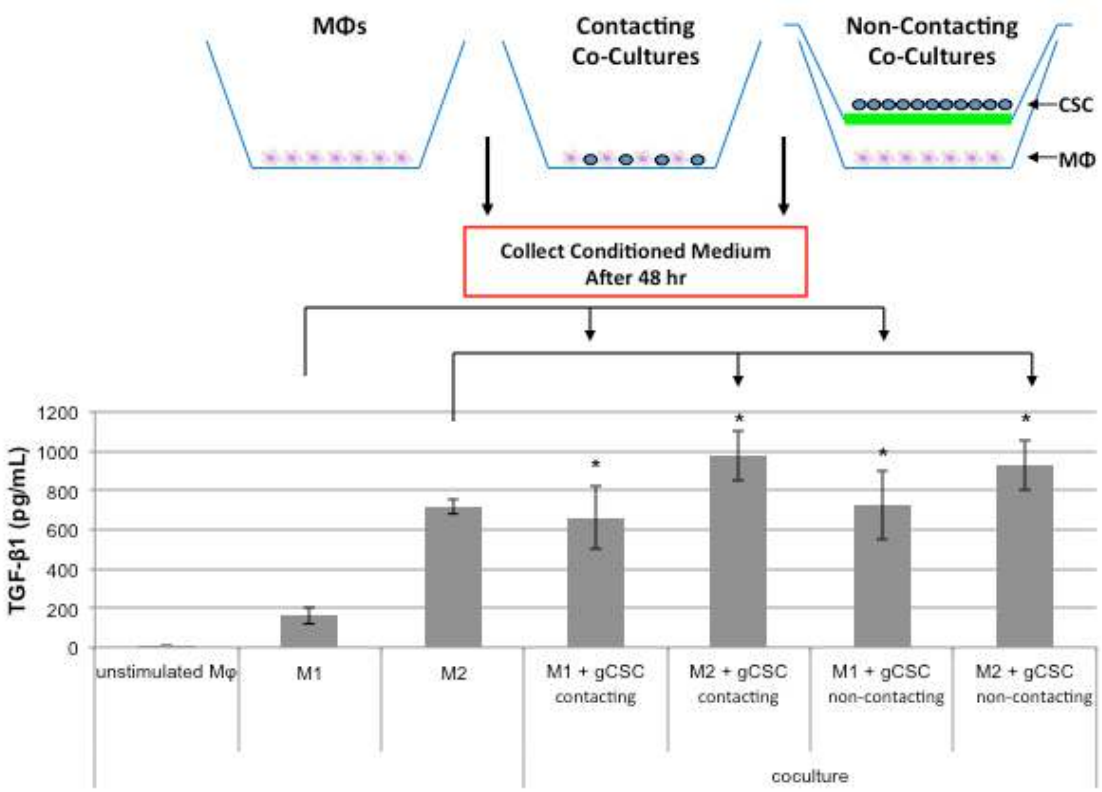


**Figure 7. CSC co-cultures influenced TGF-β1 secretion by macrophages**

**The schematic of the ELISA is shown. The supernatants of macrophage (Mϕ) cultures were collected for a TGF-β1 ELISA assay. The levels of cytokine were measured in contacting or non-contacting co-cultures of CSCs; $p<0.05$, N=3.**

To further investigate this interplay, we looked at how the presence of CSCs influence macrophage phenotype by their secretion of TGF-β1, a marker for M2 polarization. In the presence of CSCs, the levels of TGF-β1 were elevated, but the results were unaffected whether the cells were plated as contacting or non-contacting cultures (Figure 7b).

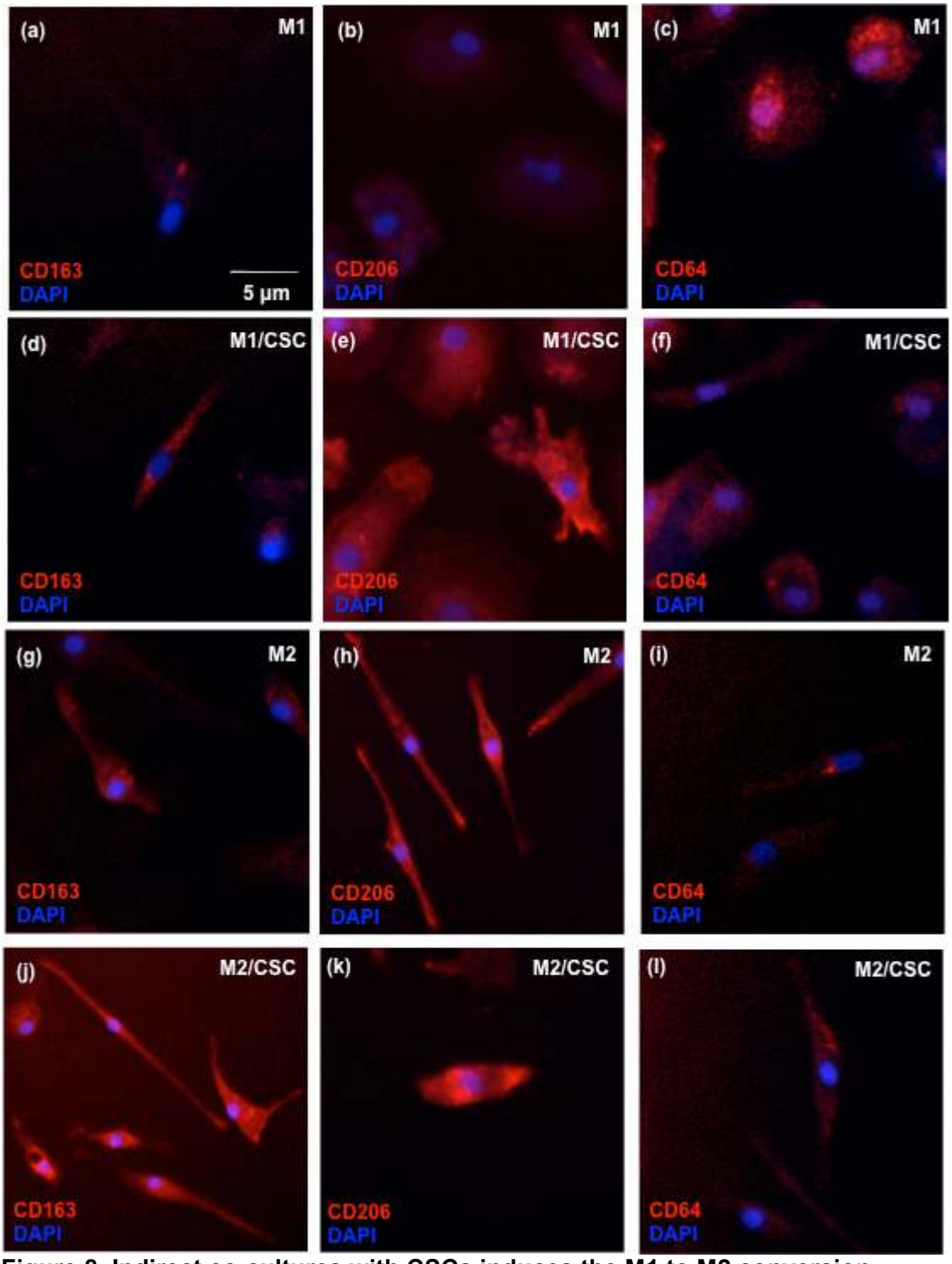


**Figure 8. Indirect co-cultures with CSCs induces the M1 to M2 conversion. Immunofluorescence images are shown of (a) – (c) M1 and (g) – (i) M2 macrophage staining as well as co-cultures with CSCs separated by a transwell chamber for (d) – (f) M1 and (j) – (l) M2 macrophages plated below. Following**

**macrophage differentiation and priming, cells were fixed and stained using CD163, CD206, and CD64 antibodies.**

The paracrine loop was further investigated in co-cultured cell models. In Figure 8, M1 or M2 macrophages were differentiated and primed as described and their respective phenotypes were confirmed by immunofluorescence staining. While CD163 and CD206 stain M2 macrophages, CD64 staining is indicative of M1 macrophages. Alternatively, monocytes were differentiated into macrophages while being co-cultured indirectly with CSCs in a transwell above. A major finding is that co-culturing indirectly with CSCs induced the conversion of macrophages from the M1 to M2 phenotype, as shown by the higher expression of M2 markers, CD163 and CD206. Thus, CSCs play an important role in modulating macrophage phenotype. CSCs not only recruit macrophages to tumors and induce M2 polarization, but are capable of converting previously M1 cells to M2 ones, thereby contributing to tumor growth and progression.

## 2.4 CONCLUSION

We were able to isolate a subpopulation of U87 cells exhibiting the CSC phenotypes of increased proliferation rate, neurosphere formation and expression of CSC markers. BTSCs also had these functions[2]. Indeed, these defining characteristics of CSCs in culture have been correlated with a poor clinical outcome in gliomas[48]. Furthermore, the CSC subpopulation exhibited an altered response to DNA alkylating agents. In co-cultures with varying proportions of CSCs, the relative viability after carmustine treatment was higher when more CSCs were present, suggesting that CSCs are more resistant. Here, we demonstrated that macrophages enhanced the migration and

degradation abilities of CSCs and BTSCs. Combined with the recently reported result that CSCs can recruit macrophages[19], this result suggests a paracrine loop. Macrophages have also been shown to influence invasion of glioma stem-like cells via TGF-β1 signaling pathway[53]. Furthermore, CSCs affect macrophages and can induce pro-inflammatory ones to display a more immunosuppressive phenotype. Thus, cells in the tumor microenvironment play an important role in cancer by interacting with tumor cells.

STAT3 plays multiple roles in tumorigenesis and response to chemotherapeutics. As STAT3 has recently emerged as a drug target for glioma and other cancers, we hypothesized that a combined carmustine and STAT3 siRNA therapy would be effective. Indeed, the viability of cells was significantly reduced over carmustine alone. The increased potency of STAT3 siRNA and carmustine combined points to a direct cellular role. While STAT3 silencing did affect response to carmustine, the magnitude was less than expected based on the role of STAT3 in vivo. These results were also observed with TMZ used instead of carmustine. This suggests that STAT3 could be mediating interactions among malignant tumor cells and other cells in the tumor milieu, specifically tumor activated macrophages. Additionally, when STAT3 was silenced, CSC migration to macrophage secreted factors was reduced. Thus, STAT3 plays multiple roles in tumorigenesis and response to chemotherapeutics. The increased potency in U87 cells of STAT3 siRNA and carmustine combined points to a direct cellular role. In addition, STAT3 silencing affects CSC or BTSC migration towards macrophage conditioned media. Thus, cell-cell communication in the tumor microenvironment may prove to be an important therapeutic target.

# 3 CHAPTER 3: DEVELOPMENT OF A CAM-LIPID COMPLEX FOR GENE SILENCING

Note: This chapter is partially reproduced from sections of the following publications:

L. Gu+, L.M. Nusblat+, N. Tishbi, S.C. Noble, C.M. Pinson, E. Mintzer, C.M. Roth, and K.E. Uhrich, 2014. Cationic amphiphilic macromolecule (CAM) – lipid complexes for efficient siRNA gene silencing. J Control Release 184: 28-35

+ Authors contributed equally

A. Gu L. prepared liposomes, performed the DLS, zeta potential, turbidity, and TEM measurements as seen in Figures 10, 11, and 12.

## 3.1 INTRODUCTION

Cationic systems involving polymers and lipids have been developed for siRNA delivery as they prevent siRNA degradation, allow siRNA endosomal escape, and silence the target mRNA[54,55]. Yet, these cationic systems have yet to overcome cytotoxicity, instability in the presence of serum, and low silencing efficiency. We previously developed cationic amphiphilic macromolecules (CAMs), which are comprised of hydrophobic acyl chains and hydrophilic poly(ethylene glycol) (PEG) chains. Within aqueous media, CAMs can self-assemble into micelles to present the PEG shell which increases the system's circulation time in the bloodstream[56]. Our group has found the alkylated mucic acid backbone to be an effective and biocompatible hydrophobic segment in applications to chemotherapeutics[57]. Two species of CAMs, differing by the

number of amine groups in their backbone (Fig. 1, 7N and 9N), were prepared previously and were shown to exhibit moderate gene-silencing efficiency with low cytotoxicity *in vitro*[58]. Thus, CAMs represent a promising delivery platform due to their self-assembly, biocompatibility, and tunable structure.

## 3.2 METHODS

### 3.2.1 MATERIALS

DOPE and DOTAP were purchased from Avanti Polar Lipid (Alabaster, AL). The anti-luciferase siRNA (sense sequence: 5′-CUUACGCUGAGUACUUCGAdTdT-3′; antisense sequence: 5′-UCGAAGUACUCAGCGUAAGdTdT-3′) and Cy5-labeled negative control siRNA were purchased from Qiagen (Valencia, CA). All cell culture media and Lipofectamine were purchased from Invitrogen (Carlsbad, CA). The Luciferase assay kit and BCA protein assay kit were purchased from Promega (Madison, WI). U87-LUC, a human primary glioblastoma cell line with constitutive expression of firefly luciferase, was generously provided by Dr. Xu-Li Wang (Pharmaceutics and Pharmaceutical Chemistry, University of Utah). All other reagents were purchased from Sigma-Aldrich (St. Louis, MO) and used as received without further purification, except where noted.

### 3.2.2 CAM-LIPID COMPLEX PREPARATION

CAMs (7N and 9N) were synthesized and characterized based on previously published procedures [17]. The calculated molecular weights of 7N, 9N, DOPE, and DOTAP are 6167, 6252, 744, and 699, respectively. Gel permeation chromatography (GPC) data of 7N and 9N are as follows: 7N (6600, PDI: 1.09) and 9N (6800, PDI: 1.11). Complexes of various CAM–lipid ratios were prepared by a co-evaporation technique as previously

described[57]. Briefly, the lipid component was comprised of a 1/1 (w/w) mixture of DOPE and DOTAP. CAM and lipid (DOPE/DOTAP) were co-dissolved in chloroform at various CAM-to-lipid weight ratios. The chloroform was removed by rotary evaporation. The resulting films were hydrated with 10 mM 4-(2-hydroxyethyl)-1-piperazineethanesulfonic acid (HEPES) buffer at pH = 7.4 overnight at room temperature. The complex suspensions were then extruded 21 times with the 100 nm pore size polycarbonate filter (Avanti Lipid, AL) through a mini-extruder (Avanti Lipid, AL) to give nanoscale CAM–lipid complexes. Formation of CAM–lipid–siRNA complexes was performed by mixing CAM–lipid formulations with siRNA for 60 min at room temperature.

### 3.2.3 ELECTROPHORETIC MOBILITY SHIFT ASSAY

CAM-lipid/siRNA complexes were prepared as previously described for CAM/siRNA complexes[58]. Dispersions were briefly vortexed and incubated for 60 min at room temperature to allow for complex formation. Prior to electrophoresis, 2 μL of 10 × BlueJuice gel loading buffer was added to each sample. Gel electrophoresis was performed using 0.8% agarose E-gels containing ethidium bromide for DNA visualization and a PowerBase electrophoretic chamber (Invitrogen, CA). Gels were imaged using BioDoc-It Imaging System (UVP, CA).

### 3.2.4 TRANSMISSION ELECTRON MICROSCOPY

A drop of CAM–lipid complex dispersion (0.05 mg/mL) with or without siRNA and a drop of uranyl acetate (0.5 mg/mL) were both dropped on a carbon film-coated copper grid. Excess solution was removed by tapping the edge of grid with filter paper. The grid was

then dried for 30 min in a desiccator at room temperature. Images were taken on a TEM-Topcon 002B (TOPOCON, Japan).

### 3.2.5 CAM-LIPID SIZE AND ZETA POTENTIAL

CAM‑lipid complexes (1 mg/mL in HEPES) with or without siRNA were analyzed using a NanoZS90 instrument (Malvern Instruments, UK) at room temperature. Each sample was run three separate times with 20 measurements per run to obtain the size and zeta potential.

### 3.2.6 CELL CULTURE

U87 and U87-LUC cells were maintained in DMEM medium supplemented with 10% fetal bovine serum (FBS) and 1% penicillin/streptomycin. Cells were incubated at 37 °C in a 5% CO2 incubator (VWR, PA). For the U87-LUC cell line, which stably expresses luciferase, expression was maintained under selective pressure by G418 (500 µg/mL).

### 3.2.7 SIRNA DELIVERY ASSAY

U87 cells were plated at a density of 5000 cells/well in 96-well plates approximately 20 h prior to transfection. Immediately prior to transfection, CAM–lipid/siRNA complexes were prepared in 20 µL of HEPES (N/P = 50). Lipofectamine was used as a positive control. A 100 nM siRNA solution was used, while CAM–lipid stock dispersions were prepared at 20 nM. An irrelevant siRNA sequence not targeted against firefly luciferase was delivered as a negative control. The CAM–lipid/siRNA complexes were brought to a total

volume of 100 μL in OptiMEM medium. The serum-containing culture medium was aspirated from the cells and each well treated with 100 μL of CAM–lipid/siRNA complexes in OptiMEM medium. After a 4 h incubation period, cells were washed 3 times with HEPES and the transfection mixture was replaced with a serum-containing growth medium and maintained under normal growth conditions. After 48 h, the cells were assayed for firefly luciferase expression using a luminometer (Turner Biosystems, WI), and the values were normalized to total protein expression using a BCA assay kit (Promega, WI).

### 3.2.8 INTRACELLULAR TRAFFICKING

U87 cells were seeded in 24-well plates at 70% confluence and allowed to adhere overnight. Uptake and release of a fluorescently labeled siRNA (Dharmacon, CO) sequence into U87 cells was evaluated using fluorescence microscopy. After 4 h or 24 h of incubation with Cy5-scrambled-siRNA (Dharmacon, CO) and 1:10 CAM–lipids, 10:1 CAM–lipids, or Lipofectamine control, U87 cells were washed twice with HEPES and stained with LysoTracker Red (Molecular Probes, OR). After fixation in 4% paraformaldehyde for 15 min and counterstaining with 4′,6-diamidino-2-phenylindole (DAPI), images were taken on an IX81 motorized inverted confocal microscope (Olympus, PA) to view siRNA localization within the cells. Colocalization of puncta was evaluated by merging images and quantifying their overlapping areas in ImageJ.

### 3.2.9 CYTOTOXICITY

The cytotoxicity of CAM-lipid complex with varying fractions of lipid and CAM was assessed with an MTS assay in U87 cells. Cells were seeded in 96-well plates for 24 h.

Following transfection with the various CAM-lipids for 4 h, cells were washed 3 times and cultured in serum-containing media. After 48 h, an MTS assay was performed and the absorbance at 450 nm was measured by a DTX880 Multimode Detector microplate reader (Beckman Coulter). Cell viability was normalized to that of U87 cells with HEPES treatment.

### 3.2.10 STATISTICS

Statistical analyses were carried out using a one-way ANOVA test with a Fisher's all-pairs post hoc comparison test (Synergy Software, PA). The significance criteria assumed a 95% confidence level ($P < 0.05$). Standard error of the mean is reported in the form of error bars on the graphs of the final data.

## 3.3 RESULTS AND DISCUSSION

While CAMs alone are promising siRNA delivery systems[58], a greater gene silencing efficiency is desirable for practical applications. Cationic lipids are the most commonly used transfection agents for gene delivery as their cationic charge can complex the anionic gene fragment and their membrane fusion properties can enhance intracellular uptake. However, lipid-based systems usually have poor stability in bloodstream and suffer relatively high cytotoxicity. As CAM delivery systems are stable in the physiological condition and cytocompatible, we hypothesized that composite complexes containing CAMs and lipids would yield a more efficient and safe siRNA delivery system.

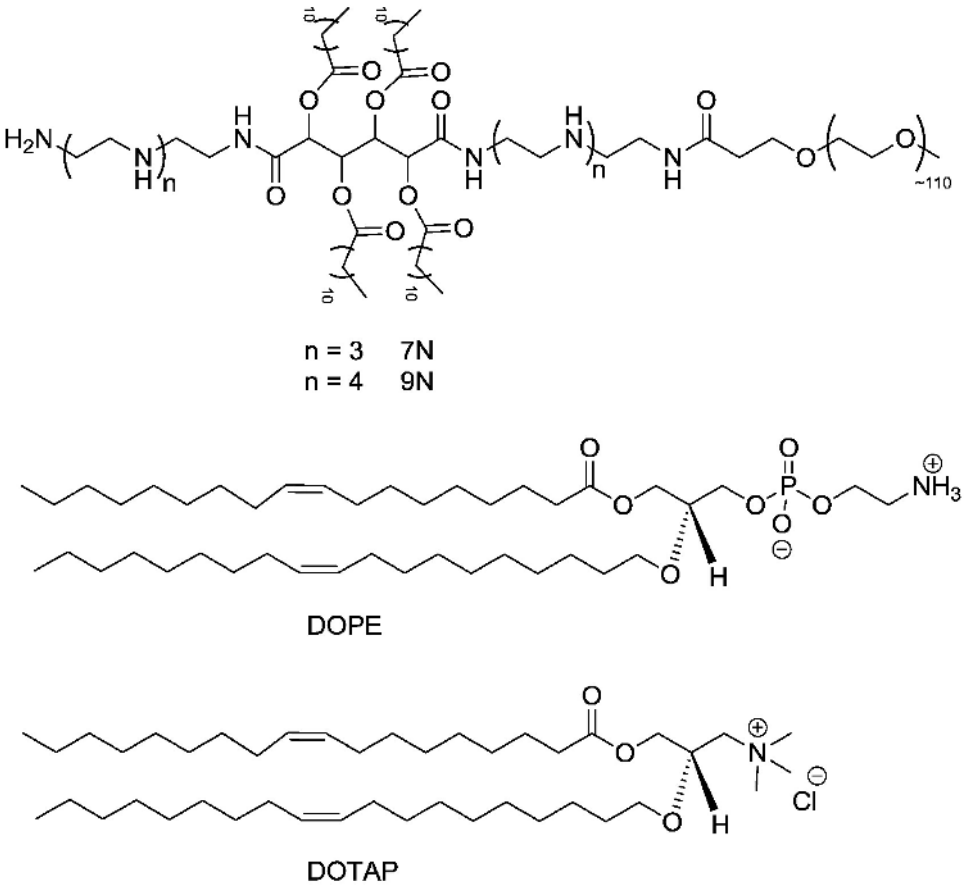


**Figure 9. Structure of CAMs**

**The structures of CAMs (7N and 9N) (top), DOPE (middle), and DOTAP (bottom) are illustrated.**

To achieve this goal, a hybrid system containing CAMs and lipids was developed using 1,2-dioleoyl-sn-glycero-3-phosphoethanolamine (DOPE) and 1,2-dioleoyl-3-trimethylammonium-propane (DOTAP) (Figure 9) at weight ratio of 1:1. DOPE was chosen for its ability to destabilize endosomal membranes and enhance siRNA release[59], while DOTAP was chosen for its high transfection efficiency due to its cationic features[60]. Complexes with varying CAM–lipid weight ratios were formulated to discern a CAM–lipid system with enhanced transfection efficiency as well as increased stability under physiological conditions. CAM–lipid complexes with various CAM to lipid weight ratios

were prepared according to a previously reported method[57]. Physical as well as biological assays of CAM–lipid complexes were performed to elucidate their efficiency as a siRNA delivery vehicle. Physical properties were evaluated by dynamic light scattering (DLS) and transmission electron microscopy (TEM), which measured the sizes and morphologies of CAM–lipid complexes, respectively. Zeta potentials were also obtained to verify the cationic surface charge, which is critical for electrostatic interactions between siRNA and CAM–lipid complexes. To evaluate their function in cells, transfection efficiency and endosomal escape of CAM–lipid complexes were evaluated using an in vitro assay with a human primary glioblastoma U87 cell line and anti-Luciferase siRNA or Cy5-scrambled siRNA.

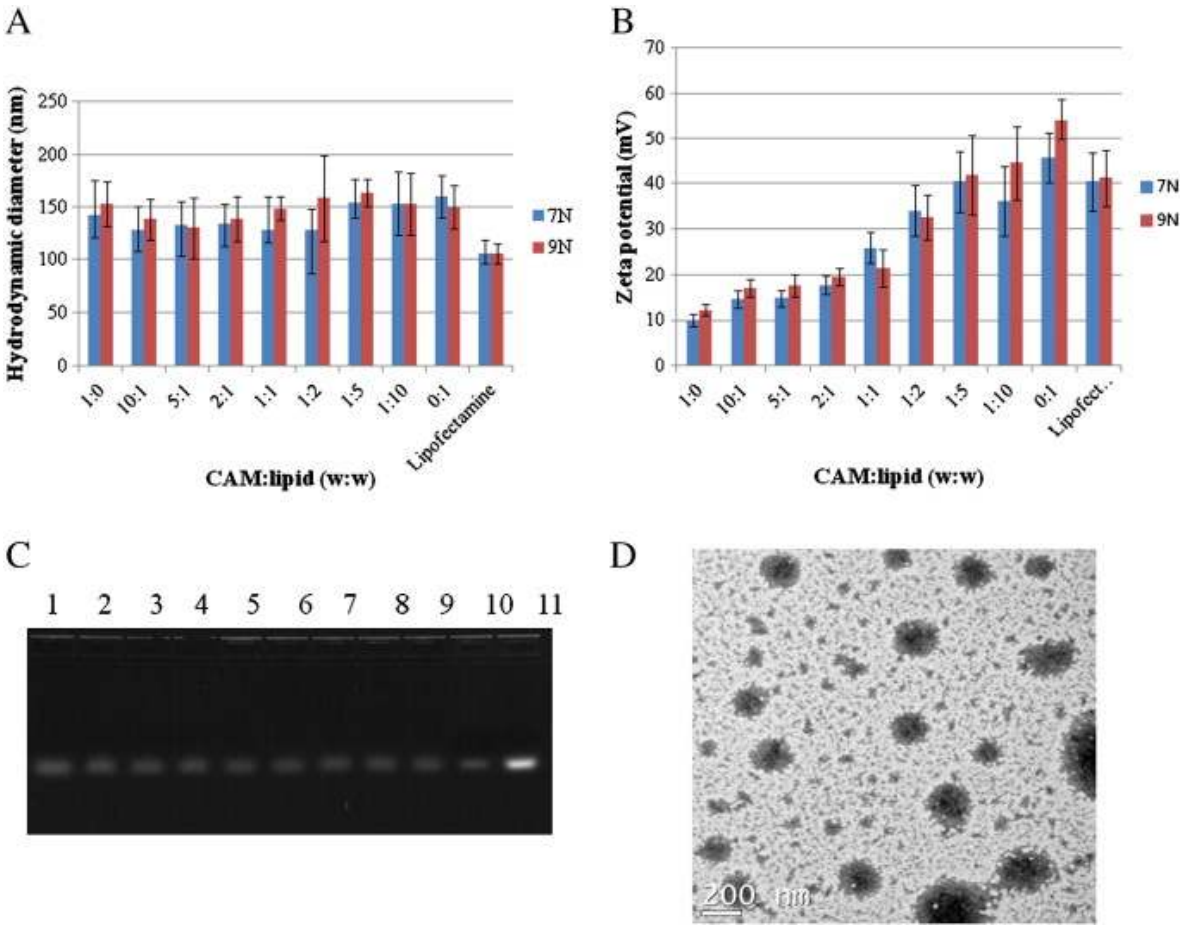


**Figure 10 CAM-lipid complex interactions**

**(A) Hydrodynamic diameter of CAM–lipid complexes in HEPES (10 mM, pH = 7.4) buffer with different weight ratios using DLS. (B) Zeta potentials of CAM–lipid complexes in HEPES (10 mM, pH = 7.4) with different weight ratios. Lipofectamine was used as control, data represent mean ± standard deviation (n = 3). (C) Electrophoresis gel, lanes 1–9 correspond to 9N–lipid weight ratios of 1:0, 10:1, 5:1, 2:1, 1:1, 1:2, 1:5, 1:10, 0:1 at N/P ratio of 50, lane 10 is Lipofectamine, lane 11 is siRNA alone. (D) TEM image of CAM (9N)-lipid at 1:1 weight ratio.**

After CAM–lipid complexes were formulated, their sizes were characterized using DLS. CAM–lipid complexes for all compositions were between 130 and 160 nm in diameter (Figure 10A), which is within the range generally considered ideal for both cellular uptake and systemic circulation[61-63]. DLS histograms showed a single peak with narrow distribution indicating that a distinct mono-dispersed complex was formed (PDI: 0.088–0.112). No aggregation was observed with any composition of the CAM–lipid complexes indicating that stable hybrid complexes were formed. CAM–lipid complex zeta potentials at pH = 7.4 varied monotonically between that for CAM alone (~ 10 mV) and for lipid alone (~ 50 mV) (Figure 10B). The zeta potential difference between CAM and lipid was due to the nature of the cationic charges. CAM possesses primary (pKa = 10.7) and secondary amines (pKa = 9.7) of which protonation may not be complete due to electrostatic repulsion and insufficient access of the aqueous media to the hydrophobic core, while DOTAP possesses the quaternary ammonium cation which is pH-independent. When forming the hybrid complexes, the PEG tail of the CAM should shield the surface charge that lower the zeta potential as increasing the CAM composition. Gel electrophoresis was used to monitor siRNA complexation with the CAM–lipid complexes. As was the case for CAMs alone[58], it was found that an N/P ratio of 50 was necessary for efficient siRNA complexation with CAM–lipid mixtures. At an

N/P ratio of 50, only a minor fraction of siRNA migrated on the gel, indicating complete complexation of siRNA to 9N–lipid for all compositions (Figure 10C). Similar results were observed when 7N–lipid was used (data not shown). TEM images of 9N–lipid complex with weight ratio of 1:1 is shown (Figure 10D). The complex size measured by TEM correlated with the DLS observations, the smaller particles observed with the hybrid complexes may be the assemblies from lipid or CAM monomer dissociated from the complexes. The CAM–lipid/siRNA complex diameters remained at approximately 100–200 nm, suggesting that the size of the nanocomplex is not affected significantly by the presence of siRNA.

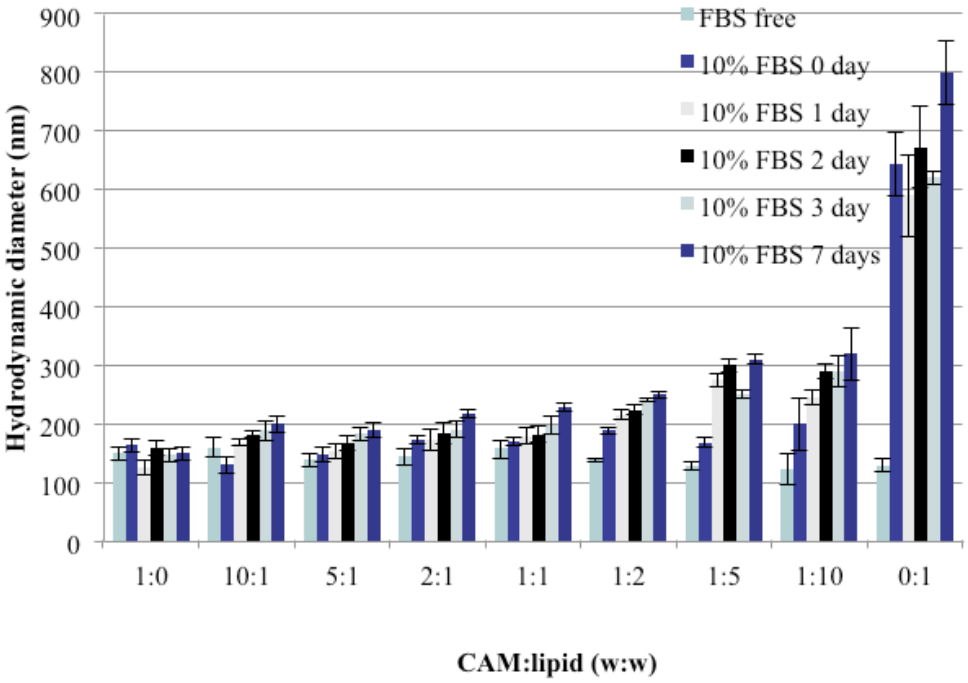


**Figure 11. Hydrodynamic diameters of CAM:lipid/siRNA complex in the presence of serum**

To further investigate the stability of the CAM–lipid/siRNA complex under serum-containing condition, the complex sizes were monitored over a week in the presence of

10% fetal bovine serum (FBS) (Figure 11). Complexes with higher CAM weight ratios maintained a 100–200 nm size range, as PEG chains of the CAM can repulse the serum proteins. When decreasing CAM weight ratios, complex sizes increased as less PEG was available on the complex surfaces. For the complexes without CAMs, immediate visual aggregation was observed with FBS addition, indicating possible damage to the siRNA caused by RNase. This data suggests that CAM–lipid complexes can maintain the integrity and protect the siRNA from degradation under the serum-containing conditions.

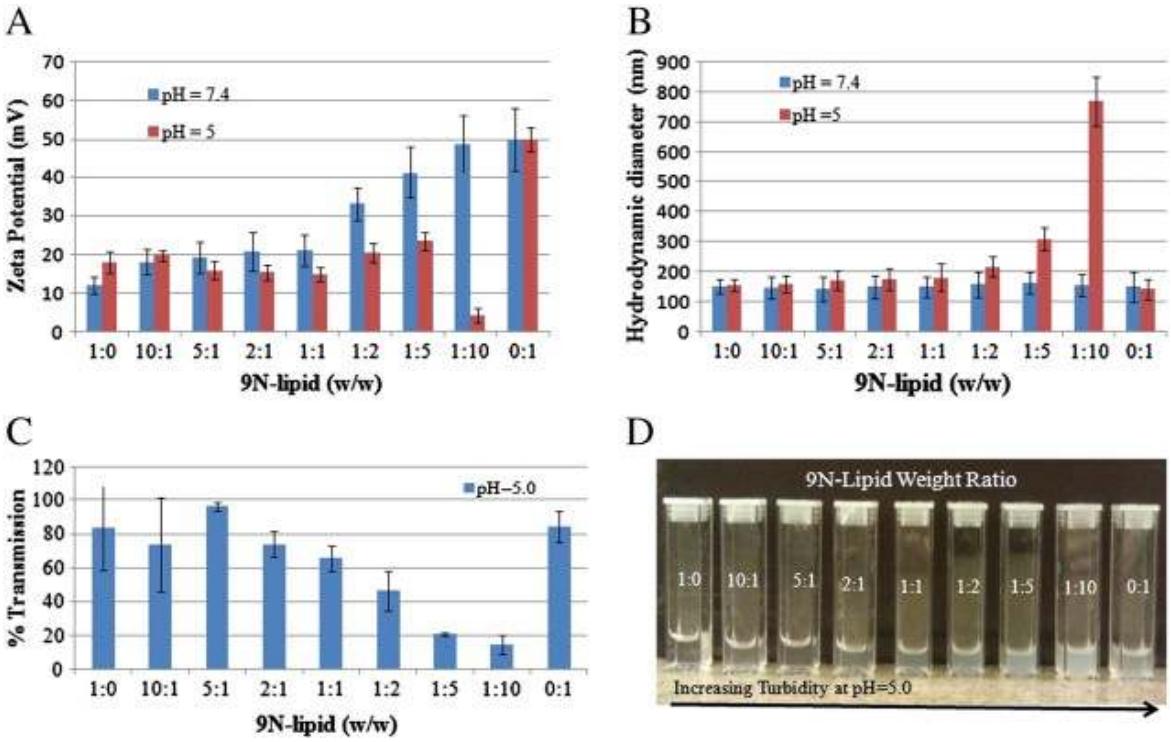


**Figure 12. Stability studies of 9N–lipid complexes**

**(A) Zeta potentials of 9N–lipid complexes at pH = 7.4 and 5; (B) hydrodynamic volumes of 9N–lipid complexes at pH = 7.4 and 5; (C) turbidities of 9N–lipid complexes at pH = 5; and (D) visual appearances of 9N–lipid complexes at pH = 5.**

To understand the differences in siRNA binding affinity at pH 7.4 and 5, zeta potentials

of 9N–lipid complexes were measured at both pH values. Zeta potentials of 9N–lipid with 1:10 weight ratio decreased drastically from 48 mV (pH = 7.4) to 5 mV (pH = 5) (Figure 12A). The descending trend of the zeta potential from pH = 7.4 to pH = 5 was also observed at 1:5, 1:2, and 1:1 weight ratios. The decreased binding affinity at pH = 5 can be anticipated by the decreased zeta potential of 9N–lipid complexes. To further study the decreased zeta potential of the complexes, sizes were measured to probe the colloidal stabilities of the complexes at pH = 5. It was shown that 9N–lipid with 1:10 weight ratio showed a steep increase from 150 nm to 770 nm (Figure 12B). Turbidities of the complexes were measured; the 9N–lipid with 1:10 ratio has less than 20% transmission (Figure 12C). Visual cloudiness in the dispersion (9N–lipid 1:1 weight ratio) suggests that precipitates form due to the complex instability at pH = 5 (Figure 12D). However, both the 9N and lipid alone were stable at pH = 5. Yet, 9N CAM has an increased zeta potential at pH = 5 compared to pH = 7.4, and when mixed with cationic lipid, the electrostatic repulsion can overcome the hydrophobic attraction leading to an instable complex that crashes out of solution. Hence, the pH-responsive effect between 9N and lipid with weight ratio 1:10 at pH = 5 was observed and further leads to the differential binding affinity between siRNA and the complexes.

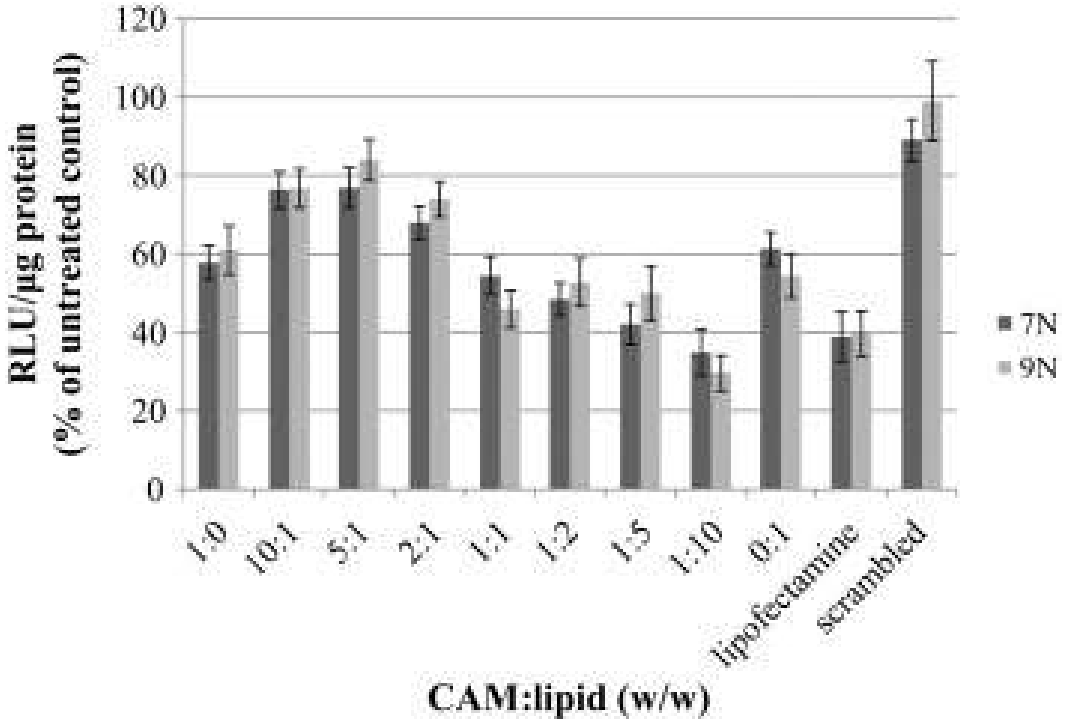


**Figure 13. Gene silencing of CAM-lipids**

**Luciferase reporter gene down-regulation assay performed over 48 h performed with the U87 luciferase cell line using complexes formulated from CAM–lipid complexes and anti-luciferase siRNA at N/P ratio of 50. Lipofectamine is used as a control. Data represent mean ± standard error (n = 3).**

To evaluate the gene silencing efficiency of CAM–lipid systems, the delivery of anti-luciferase siRNA to U87-Luc cells expressing luciferase was monitored. Nearly no silencing was observed with a scrambled siRNA control, indicating that the gene knockdown was specifically induced by anti-luciferase siRNA alone. Similar transfection efficiencies were found at 60% for both CAM alone and lipid alone (Figure 13). CAM–lipid complexes with weight ratios of 10:1, 5:1, and 2:1 showed decreased transfection efficiencies compared to the CAM or lipid alone. In contrast, the transfection efficiencies of CAM–lipid complexes with weight ratios of 1:1, 1:2, 1:5, and 1:10 were improved and

comparable to Lipofectamine. The transfection efficiency trends reveal that increasing CAM ratio in the CAM–lipid complex yields decreasing transfection efficiency. Based on intensive literature precedence, increasing CAM ratios likely yield higher PEG coating percentages in the CAM–lipid complex which eventually impede the cellular uptake of the complex[57]. However, CAM alone showed higher efficiencies than the CAM–lipid complexes with weight ratios of 5:1, 2:1, and 10:1. This result suggests that the CAM–lipid complex is not simply a mixture of polymer and lipid systems; synergistic effects between the polymer and lipid appear to play an important role in the delivery process. As further support, CAM–lipid complexes with weight ratios of 1:1, 1:2, 1:5, and 1:10 gave enhanced transfection efficiencies compared to CAM or lipid alone. These formulations also had comparable efficiency to Lipofectamine. We postulate that CAM–lipid complexes possess a unique micelle-liposome mixed structure, which requires additional detailed investigations. To examine the synergistic effect between CAM and lipid and to gain mechanistic insights, sequential studies were carried out using 9N–lipid with a weight ratio of 1:10, as the 9N–lipid with 1:10 ratio showed higher transfection efficiency than other formulations.

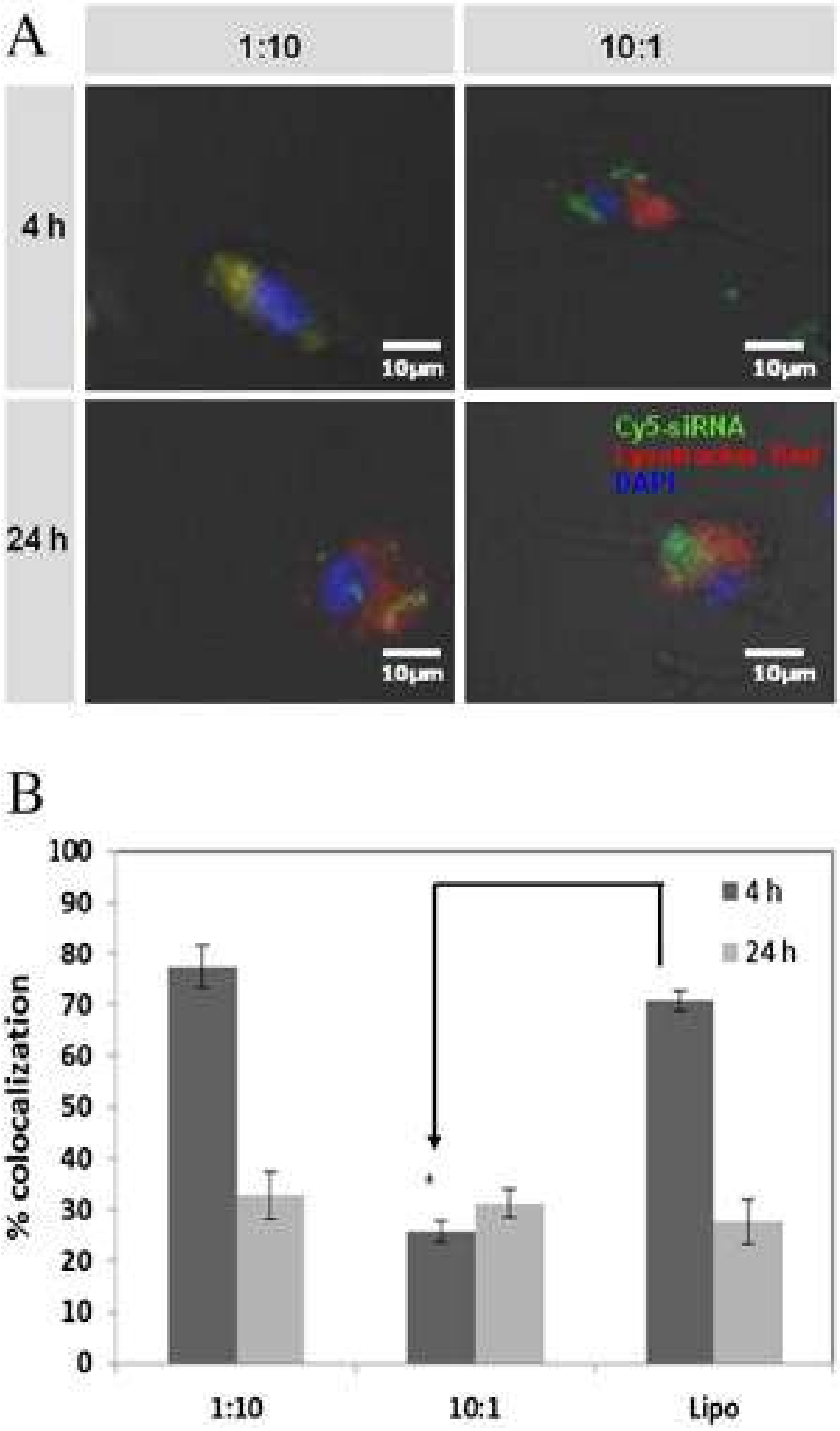


**Figure 14. Endosomal escape of complexes**

**(A) Confocal microscope images of Cy5-siRNA (green) and endosomal (red) distribution in U87 cells when delivered by the indicated 9N–lipid complexes, at 4**

**h (top panel) and 24 h (bottom panel) post-transfection. (B) Colocalization of puncta was quantified using ImageJ. The percent colocalization of Lysotracker Red and Cy5-siRNA puncta was calculated as mean gray value from colocalized points divided by mean gray value from sum of points using Image J. Data represent mean ± standard error; $p<0.05$, N=3.**

To further investigate the endosomal escape of siRNA delivery, intracellular trafficking of 9N–lipid was examined using confocal microscopy. 9N–lipid/Cy5-siRNA (9N–lipid weight ratio 1:10) was co-localized with LysoTracker Red after 4 h of incubation (Figure 14). This observation suggests that the complexes were internalized but had not yet been released from endosomes or early lysosomes by 4 h. After 24 h, only minimal co-localization was observed and more extensive siRNA distribution was observed in the cytoplasm (data not shown), suggesting that Cy5-siRNA had undergone endosomal/lysosomal escape. Based on the previous pH-dependent data, the endosomal escape could be explained by the pH-responsive feature of the 9N–lipid at weight ratio of 1:10. When the complexes are internalized in endosomes, the collapse of the complexes at acidic pH caused the release of lipid, CAM, and siRNA. The lipid can serve as a destabilizing agent to disrupt the endosome membrane[64]. The CAM can induce endosome disruption via the well-studied proton sponge theory[65,66]. The siRNA is then released into the cytoplasm to trigger the RNAi process after the endosomal disruption. The same trends were observed when using Lipofectamine as the carrier. For the less effective carrier (9N–lipid with weight ratio of 10:1), siRNA appeared to aggregate on the cell surface after 4 h. After 24 h, some CAM–lipid complexes were internalized, however, much more CAM–lipid complex remained on the cell surface as compared to the 1:10 formulation. These results suggest that siRNA efficiency is impaired at 10:1 weight ratio due to insufficient cell uptake and decreased intracellular

release of siRNA.

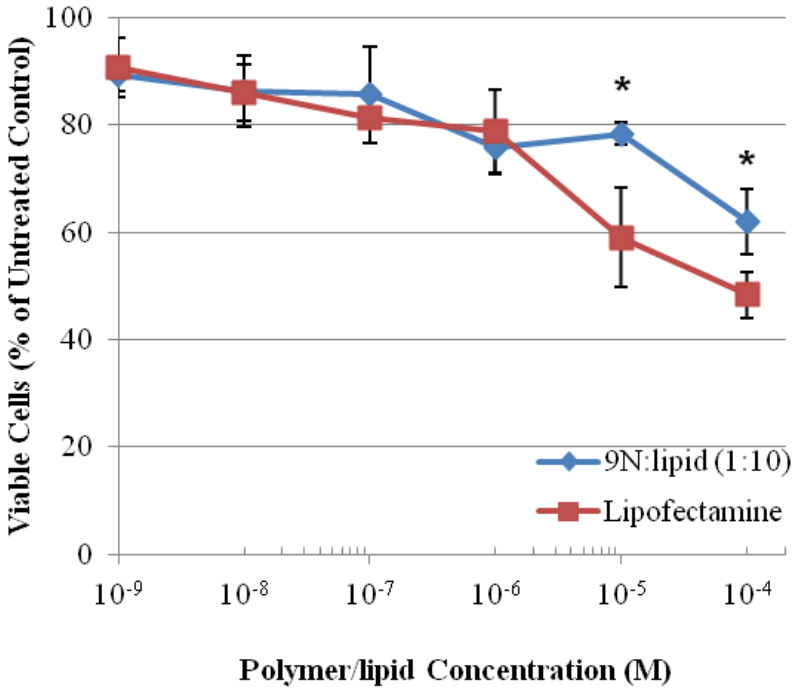


**Figure 15. Cytotoxicity of CAM-lipids**

**Cytotoxicity of 9N-lipid/siRNA (1:10 w/w) complexes was compared to Lipofectamine/siRNA in U87 glioma cells after 72 h of exposure. Data represent mean ± standard error. Asterisks represent concentrations at which CAM-lipid complexes elicited a significantly lower cytotoxicity than Lipofectamine; $p < 0.05$, N=3.**

Therefore, to assure CAM–lipid complexes of optimized composition have great potential to be used as efficient non-viral carriers for siRNA delivery, cytotoxicity studies were conducted. Low cytotoxicity of the CAM–lipid complexes was observed (Figure 15).

## 3.4 CONCLUSION

We developed a novel complex that combines polymer and lipid to effectively delivery siRNA. Size and zeta potential measurements validated that CAM–lipid complexes are suitable for siRNA complexation and delivery. *In vitro* siRNA delivery experiments demonstrated that CAM–lipid complexes with specific CAM–lipid weight ratios have comparable gene silencing efficiencies compared to Lipofectamine control. Further, intracellular trafficking revealed that siRNA can escape from endosomes and are released from CAM–lipid complexes to down-regulate genes.

Thus, these CAM–lipid complexes exhibit marked advantages compared to prior developed systems. While most delivery systems that achieve delivery of nucleic acids do so at the cost of high cytoxicity, in contrast, here we have developed a system with good performance and low cytotoxicity. Notably, the ability to mediate gene silencing appears to be at least partially due to the pH-dependence of the interaction between the CAM–lipid complexes and the siRNA. Here, we showed the mechanism of differential binding affinities of siRNA to the complexes at pH = 7.4 and 5, namely, those complexes were unstable under acidic conditions. The pH-responsive feature of the complexes appears to be a natural feature of the components that we designed and does not require additional complications such as attachments of endosomal disruption peptide or reducible disulfide bonds. These studies strongly suggest that CAM–lipid complexes can serve as efficient siRNA delivery vehicles and provide a novel method to probe delivery mechanisms.

# 4 CHAPTER 4: SILENCING HYPOXIA MEDIATORS

## 4.1 INTRODUCTION

The tumor microenvironment of GBM is a complex tissue of cells, including astrocytes, macrophages, pericytes, fibroblasts, and endothelial cells. Macrophages play a crucial role in the immune response. Yet, due to signaling by CSCs, macrophages undergo a switch towards an immunosuppressive state, promoting angiogenesis, reducing phagocytosis, and inhibiting T-cell proliferation[19]. Additionally, inherent characteristics within CSCs increase a tumor's resistance against chemotherapeutic agents including temozolomide[67]. As such, novel treatments targeting this tumor subset are of paramount importance. Hypoxia associated factors, such as HIF-2α, are highly expressed in CSCs in some cancers[68], resulting in a hypoxic state. HIF-2α enhances the production of genes involved in maintaining the stem-like properties of these cells, and it is specifically overexpressed in CSCs, enhancing proliferation. HIF-2α also plays a role in metastasis by promoting angiogenesis.

Based on this knowledge, we hypothesize that since HIF-2α mediates the effects of hypoxia on CSCs, its silencing would decrease CSC functions and reduce the stemness within the tumor. HIF-2α silencing will presumably have the most potent effect on CSC functions under hypoxic conditions since that is when HIF-2α is overexpressed. If HIF-2α can successfully decrease CSC functions, we hope that when used in combination with TMZ, it would significantly reduce tumor recurrence and allow for a better survival rate.

## 4.2 METHODS

### 4.2.1 CHEMOTHERAPEUTIC EFFECT OF HIF-2α SIRNA

CSC and BTSC neurospheres were prepared as described in chapter 2. For experiments mimicking hypoxic conditions, cells were cultured with 100μM deferoxamine mesylate (Sigma-Aldrich), a hypoxia mimetic. A Silencer Select siRNA against human HIF-2α (Dharmacon) was delivered to cells using Lipofectamine RNAiMAX as described by the manufacturer (Invitrogen). Silencer Select Negative Control siRNA (Invitrogen) was used as a control, nontargeting sequence. After 24 h, 1μM TMZ (Life Technologies) was added to the media. After 48 h, an MTT assay (Promega) was performed to evaluate viability as a measure of chemotherapeutic response to a combined HIF-2α siRNA and temozolomide therapy.

### 4.2.2 WESTERN BLOTTING

Western blots were done of whole cell lysates from macrophages transfected with HIF-2α siRNA primed with either LPS or IL-4, and cytoplasmic extracts of U87s and CSCs treated with +/- 100μM deferoxamine mesylate (DFX) (Sigma-Aldrich) for 24hrs. Complete Mini EDTA-free protease inhibitor cocktail (Roche) was used to prepare whole cell lysates in RIPA buffer. Lysates were run on an 8% acrylamide gel at 100V until the dye front passed through the stacking layer and subsequently, at 150V until the dye front reached the bottom of the gel. Precision Plus Protein standard (Bio-Rad) was used as a molecular weight ladder. The gel was transferred onto a nitrocellulose membrane for 1 h at 100V and blocked in 5% BSA in TBST for 1 h. The membranes were incubated in primary antibody overnight at 4°C on a shaker in blocking buffer. Western blotting was performed using a rabbit anti-HIF-2α antibody (ab199) (Abcam) at 1:500 and rabbit anti-GAPDH (14C10) (Cell Signaling) as the housekeeping gene. After washing 3 times for

10 min in TBST, blots were incubated in HRP-conjugated secondary antibodies for 1h at RT on a shaker. After washing 3 times for 10 min in TBST, membranes were incubated in SuperSignal West Pico Chemiluminescent Substrate for 5 min and exposed to film for 5 and 10min.

### 4.2.3 MIGRATION ASSAY

Transwell filter chambers with 8 μm pores (BD Biosciences) were used in a 24-well plate for the migration assay. U87, CSCs, or BTSCs (700,000 cells/350 μl) within DMEM/F12 medium were seeded into the upper well of the insert, while the lower well contained 600 μl of LPS or IL-4 stimulated macrophage conditioned media, LPS or IL-4 supplemented macrophage media, or unconditioned macrophage media (RPMI, 10% FBS, 1% P/S, and 4mM L-glutamine). Chambers were incubated at 37 °C and the cells were allowed to migrate for 24 h. The outer side of the insert was gently rinsed with PBS prior to imaging. Migrated cells were counted under a light microscope in 10 randomly chosen fields in the bottom well with 10× objective. At least 50 cells were analyzed per experiment. All other co-culture experiments were done using 4 μm pore size transwell chambers (BD Biosciences).

### 4.2.4 EXTRACELLULAR MATRIX DEGRADATION

CSCs were plated on a DQ-collagen IV (Invitrogen) thin film overnight. Since the matrix is fluorescently labeled, degraded areas were indicated by the presence of fluorescence within the cells. Fluorescent areas, indicating areas of degradation, were quantified in Image J and normalized to total cell area.

### 4.2.5 IMMUNOFLUORESCENCE OF SPHEROIDS

Spheroids of U87 cells were grown for 3 days using the hanging drop method. Each droplet contained 20,000 cells in 20 µl media. Each spheroid was plated into a well of a 96-well plate containing 50 µl of 2% agarose in PBS after waiting 5 min for the gel to solidify. The wells were filled with 100 µl media. After 24 h, the spheroids became smaller and tightly packed. Neurospheres of CSCs were prepared by culturing in NSC media, as described in chapter 2. Spheroids were cryosectioned in 20 µm slices, stained, and then imaged by confocal microscopy in Lab-tek chambers (Thermo Scientific). Cells were stained with Nestin (ab6320) (Abcam) and CD133 (PAB12663) (Abcam) for neural stem cell markers, and GFAP (BT-575) (Biomedical Technologies Inc.), βIII-tubulin (Sigma-Aldrich), and MBP (Abcam) were used as markers of differentiated cells. DAPI (Invitrogen) was the nuclear stain used.

### 4.2.6 STATISTICS

The data is presented as means ± standard error of the mean (SEM). Each experiment was repeated three times and comparisons were done using one-way ANOVA and post-hoc analysis, as indicated in the figures.

## 4.3 RESULTS AND DISCUSSION

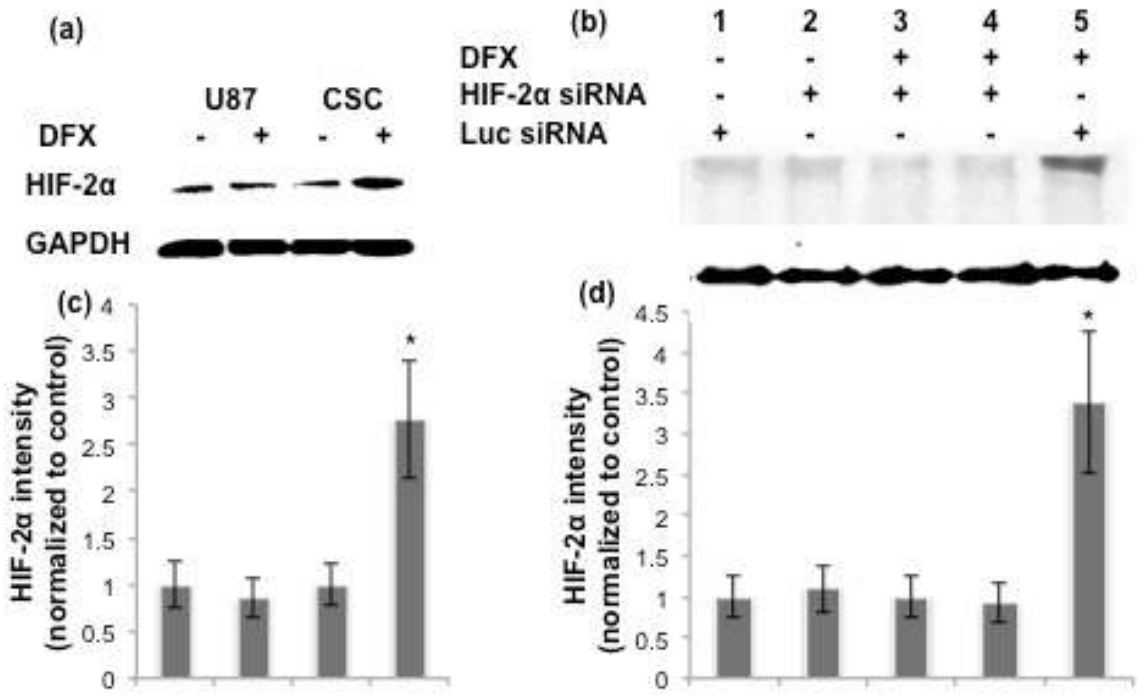


**Figure 16. HIF-2α expression in CSCs**

**Representative immunoblots of whole cell lysates are shown. Blots were probed for HIF-2α and GAPDH was used as a housekeeping gene to normalize for protein loading. (c) Bar graphs are shown obtained by densitometric analysis of western blot data. Results (mean±S.E.M.) represent the ratio between HIF-2α and GAPDH levels, and are normalized to (a) untransfected or (b) Luc siRNA; $p<0.05$, N=2.**

Figure 16a shows the expression levels of HIF-2α in U87 and U87-derived CSCs under hypoxia and normoxia conditions. Hypoxia was mimicked using deferoxamine mesylate (DFX). In a hypoxic environment, the CSC population is enriched and overexpresses HIF-2α, while levels under normoxia culturing conditions are low for both U87 and CSC cells. Quantification of bands and normalization to GAPDH revealed that CSCs expressed 2.5-fold increase HIF-2α of levels when treated with the hypoxia mimetic, DFX. Figure 16b shows HIF-2α silencing of normoxic and hypoxic U87-CSCs. We

show that HIF-2α is effectively silenced in cells under normoxia and using DFX. Lane 4 contains HIF-2α silenced CSCs using our CAM-lipid micelle delivery system developed, as discussed in chapter 3. All other lanes were transfected with Lipofectamine RNAiMAX. There was approximately a 3.5-fold decrease in HIF-2$\alpha$ expression when transfected with siRNA. As depicted, the CAM-lipid micelle system was equally effective at HIF-2α silencing of CSCs.

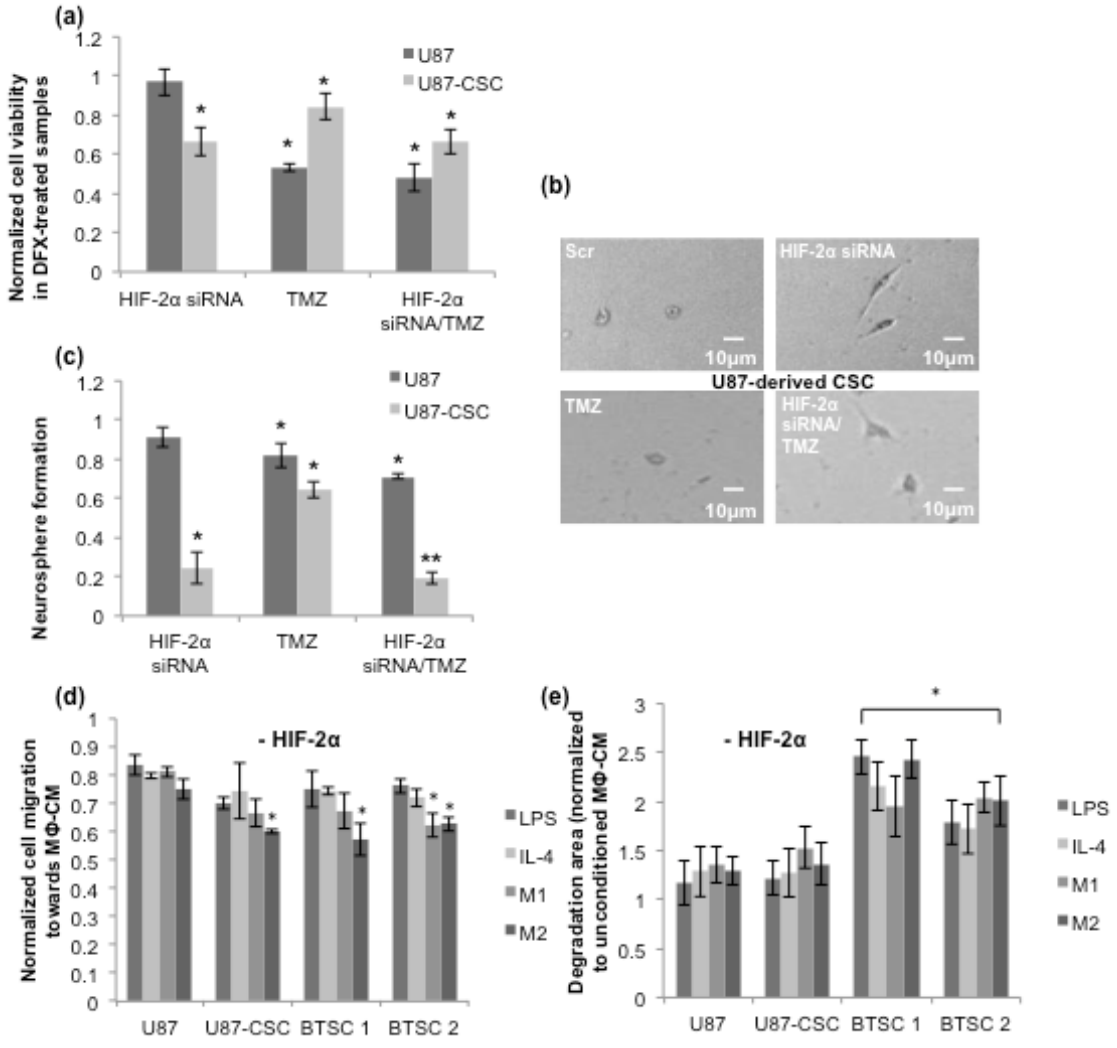


**Figure 17. HIF-2α silencing reduces chemoresistance of CSCs**

**(a) Viability was assessed of HIF-2α silenced or a non-targeting control siRNA treated CSCs at 48h following incubation with the hypoxia mimetic, DFX, and the DNA alkylating agent, TMZ; $p<0.05$, N=3. (b) Phase immunofluorescence of HIF-2α and/or TMZ treated CSCs is shown. (c) Neurosphere formation in the presence of DFX after 7 days following a 48h treatment with HIF-2α and/or TMZ; *$p<0.05$, **$p<0.01$, N=3. Data was normalized to cells treated with a non-targeting control siRNA. (d) The graph shows fold increase of cell migration over the non-conditioned medium treated cells. At least 50 cells per field and 10 fields were counted (10X) of cells that migrated through the transwell. Statistics compare the respective conditions to U87 cells; *$p<0.05$, N=3. (e) U87s, CSCs, or BTSCs plated on a DQ-collagen IV thin film and co-cultured in macrophage conditioned media or LPS or IL-4 supplemented media. Fluorescent areas (degraded areas) were quantified in Image J and normalized to total cell area. Statistics were done comparing the respective conditions to U87 cells; *$p<0.05$, N=3.**

The silencing of HIF-2α exerts distinct effects on the responsiveness of CSCs to DNA alkylating chemotherapeutics. U87 or CSCs were treated with TMZ and/or HIF-2α siRNA. TMZ drastically reduces viability of U87 cells, but the CSC sub-population is only slightly reduced by TMZ (Figure 17a). HIF-2α silencing slightly decreases viability of CSCs and also has an additive effect with TMZ to produce modest reductions in viability under the conditions studied. The effect of HIF-2α silencing is most pronounced at 48 h following transfection, which corresponds to maximal siRNA silencing. Phase immunofluorescence of treated cells are shown in Figure 17b. We observed that CSCs treated with HIF-2α siRNA exhibited a more spread morphology, which is often indicative of a more differentiated state. More dramatic is the 80% decrease in neurosphere

formation of HIF-2α silenced CSCs with or without administration of TMZ (Figure 17c). Thus, HIF-2α plays a large role in mediating CSC stemness. Additionally, the migration and degradation abilities of CSCs and BTSCs are markedly decreased when HIF-2α is silenced, but this effect was not as pronounced in U87s (Figure 17d and 17e).

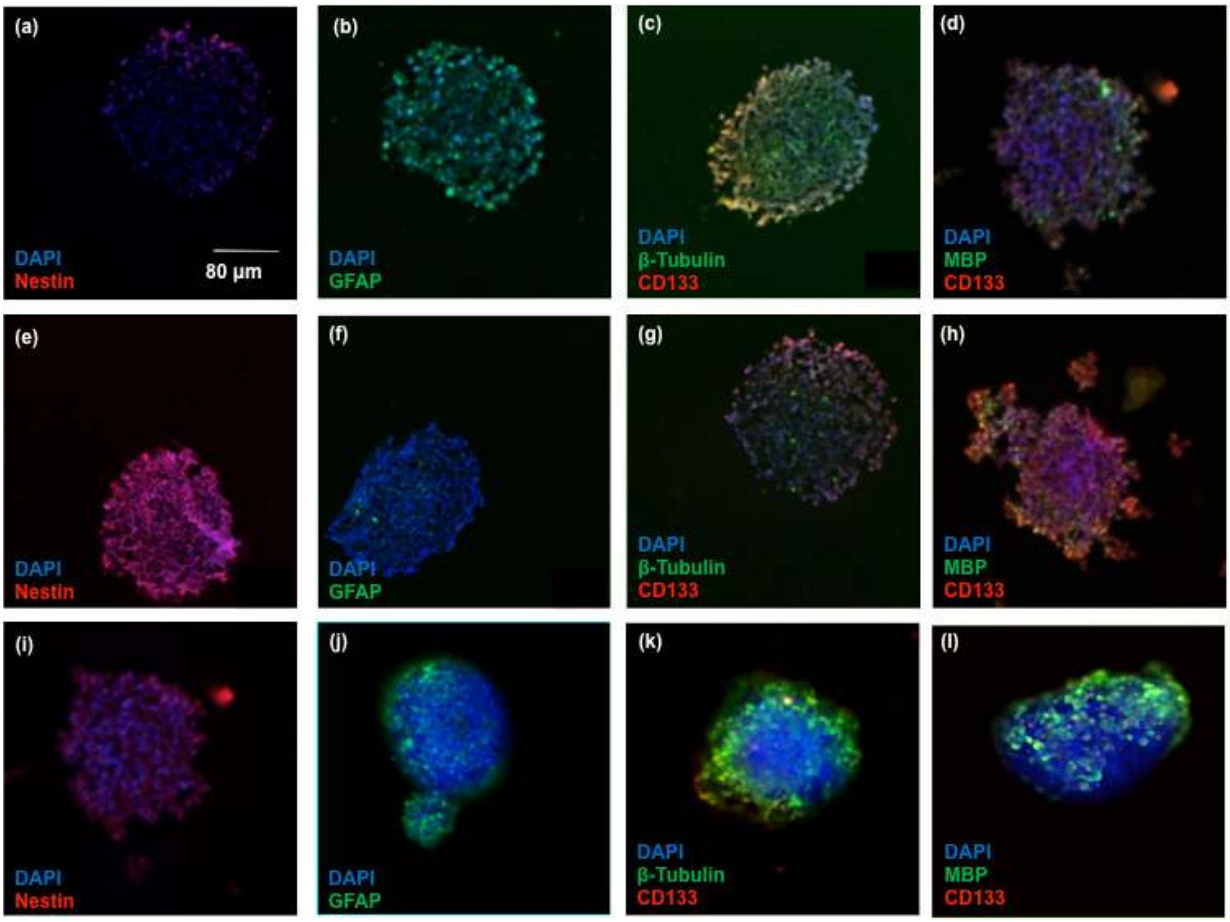


**Figure 18. HIF-2α silenced CSC neurospheres display differentiation markers**

**The illustrations depict cryosections of U87 spheroids in (a) - (d), while CSC neurospheres are in (e) - (h), stained for stem and differentiated cell markers. For HIF-2α silenced spheroids depicted in (i) - (l), CSC neurospheres were treated with DFX following HIF-2α silencing for 48 h and cryosections were imaged. Cells were stained with Nestin and CD133 for neural stem cell markers, and GFAP, β-tubulin, and MBP were used as markers of differentiated cells. DAPI was the nuclear stain**

**used.**

To further elucidate the role of HIF-2$\alpha$ on CSC stemness, spheroids were prepared using the hanging drop method or by culturing in NSC media with U87 or CSC cells, respectively. To examine the differentiation behavior in greater detail, neurospheres treated with the hypoxia mimetic, DFX, and HIF-2α siRNA were stained with antibodies to several stem cell and differentiation markers (Figure 18). Nestin and CD133 staining was indicative of stem cells, while GFAP, β-tubulin, and MBP marked differentiated cells. Here, we further illustrate that HIF-2α siRNA treatment reduces CSC stemness effectively, due to the increased expression of differentiated cell markers following treatment. While these images were taken 48 h following transfection, it is speculated that expression of differentiation markers would disrupt the intactness of the spheroid and dissociate. However, at this timepoint, the effect was not observed. This further confirms our result that HIF-2α silencing strongly induces differentiation and may be an important molecule for targeting applications.

### 4.4 CONCLUSION

There has recently been an increase in the amount of research done pertaining to cells crucial to the microenvironment of solid tumors. By understanding the intercommunication done between macrophages, CSCs, and differentiated cancer cells, one can choose to target different aspects of the tumor in order to effectively treat the tumor. Additionally, by learning more about pathways specific to CSCs, targeted treatments could be effectively developed.

## 5 CHAPTER 5: CONCLUSION

## 5.1 KEY FINDINGS

CSCs are important in macrophage polarization, but the reciprocal effect of macrophages on the CSC phenotype is unclear. We hypothesized that macrophages can enhance CSC proliferation, neurosphere formation, chemotherapeutic resistance, migration, ECM degradation, and cytokine secretion. In this dissertation, we demonstrated that M2 macrophages derived from peripheral blood monocytes enhanced CSC functions, and that this occurred via TGF-β1 signaling. Groups reported that juxtacrine signaling is involved in STAT3 activation and direct co-cultures enhanced expression of STAT3 in glioma bulk tumor cells[44]. In contrast, here we focused on the CSC population specifically and showed that a paracrine loop is involved in CSC signaling. Specifically, we showed that culture in the proximity of CSCs upregulates TGF-β1 production in macrophages and induced M2 polarization. In turn, in the presence of conditioned media from M2 macrophages, CSCs exhibited increased migration. Thus, there exists a bidirectional cross talk between CSCs and macrophages that results in increased invasiveness and migration of CSCs. Furthermore, we show that siRNA mediated silencing of STAT3 reduced the chemoresponsiveness and migratory abilities of the CSCs. This is consistent with literature on bulk tumor cells demonstrating that silencing of STAT3 inhibits the growth of tumor cells and induces apoptosis. Thus, the signaling among cells in the tumor microenvironment plays an important role in tumor growth, motility, and therapeutic resistance.

To better deliver siRNA to tumors, a novel system was co-designed for gene silencing applications. This entailed adding lipids to a CAM micelle, based on the hypothesis that a mixed micelle-lipid nanocomplex would exhibit pH-dependent instabilities that could promote endosomal escape. Our results showed that this delivery system leads to

efficient uptake of siRNA within tumor cells and their subsequent pH-dependent release from endosomes. This system was then validated for HIF-2α silencing in hypoxic CSCs. Hypoxia plays a key role in maintaining the stemness of the CSC population through HIF-2α, an important transcriptional effector in hypoxic tumors. HIF-2α silencing under hypoxia reduced CSC functions, and its effects were additive with existing DNA alkylating combination treatments. Thus, silencing hypoxic mediators where these cells reside or disrupting the signaling between macrophages and CSCs may have therapeutic potential.

## 5.2 FUTURE WORK

Further work is needed to identify other molecular regulators of CSCs in the hypoxic niche that point to specific signaling mechanisms for targeting them. Other strategies could target macrophages since they are a predominant stromal cell type within glioblastoma. Since it has been established that the cross talk is crucial in tumorigenesis, reducing the immunosuppressive macrophage phenotype or their ability to respond to CSC chemokines such that they form the antitumor (M1) phenotype might be effective.

Also, attaching targeting ligands to the developed micelle system may be useful in applying the system clinically for efficient siRNA delivery in tumors. Using the pH-sensitive delivery system, the micelles could be functionalized to specifically target CSCs and/or macrophages, which would subsequently starve tumor cells. These micelles could contain encapsulated chemotherapeutic drugs, such as doxorubicin, to kill bulk tumor cells as well. The delivery of doxorubicin within liposomes has already been

shown to improve its distribution[69], leading to improved dosing for reducing cardiovascular toxicity and promoting antitumor effects. Due to the leaky vasculature and lack of lymphatics, both targeted and untargeted micelles accumulate passively in tumors. Currently, clinical studies have focused on targeting the EGFR pathway[70], but other targeted formulations may be an important treatment strategy.

## 5.3 LIMITATIONS

Some limitations to the applications of siRNA technology is that uptake within tumors is mitigated by diffusion kinetics of STAT3 siRNA. The issue of drug uptake within the tumor interior is also problematic *in vivo*[71]. Additionally, some limitations to the strategy of targeting are off-target effects to sequences that are partially complementary. Also, since multiple cell types express STAT3, its silencing could result in toxicity. By conjugating a ligand to the micelle surface may increase uptake by the RES, despite PEGylation. Immune cells might attack the ligand-conjugated micelles, resulting in an immune reaction[72,73]. A small peptide or $F_v$ fragment may extend the liposome circulation time for improved delivery to target tumor tissues. Additionally, other signaling molecules may compensate during tumor progression.

## 5.4 REFERENCES


1. Li, Z. et al. Immunotherapy targeting glioma stem cells--insights and perspectives. *Expert Opin Biol Ther* **12**, 165-78 (2012).

2. Hemmati, H.D. et al. Cancerous stem cells can arise from pediatric brain tumors. *Proc Natl Acad Sci U S A* **100**, 15178-83 (2003).

3. Ortensi, B., Setti, M., Osti, D. & Pelicci, G. Cancer stem cell contribution to glioblastoma invasiveness. *Stem Cell Res Ther* **4**, 18 (2013).

4. Heddleston, J.M. et al. Glioma stem cell maintenance: the role of the microenvironment. *Curr Pharm Des* **17**, 2386-401 (2011).

5. Kolenda, J. et al. Effects of hypoxia on expression of a panel of stem cell and chemoresistance markers in glioblastoma-derived spheroids. *J Neurooncol* **103**, 43-58 (2011).

6. Li, Z., Wang, H., Eyler, C.E., Hjelmeland, A.B. & Rich, J.N. Turning cancer stem cells inside out: an exploration of glioma stem cell signaling pathways. *J Biol Chem* **284**, 16705-9 (2009).

7. Wang, R. et al. Glioblastoma stem-like cells give rise to tumour endothelium. *Nature* **468**, 829-33 (2010).

8. Graeber, M.B., Scheithauer, B.W. & Kreutzberg, G.W. Microglia in brain tumors. *Glia* **40**, 252-9 (2002).

9. Leek, R.D. & Harris, A.L. Tumor-associated macrophages in breast cancer. *J Mammary Gland Biol Neoplasia* **7**, 177-89 (2002).

10. Charles, N.A., Holland, E.C., Gilbertson, R., Glass, R. & Kettenmann, H. The brain tumor microenvironment. *Glia* **60**, 502-14 (2012).

11. Green, C.E. et al. Chemoattractant signaling between tumor cells and macrophages regulates cancer cell migration, metastasis and neovascularization. *PLoS One* **4**, e6713 (2009).

12. Hao, N.B. et al. Macrophages in tumor microenvironments and the progression of tumors. *Clin Dev Immunol* **2012**, 948098 (2012).

13. Vasievich, E.A. & Huang, L. The suppressive tumor microenvironment: a challenge in cancer immunotherapy. *Mol Pharm* **8**, 635-41 (2011).

14. Dijkgraaf, E.M. et al. Chemotherapy alters monocyte differentiation to favor generation of cancer-supporting M2 macrophages in the tumor microenvironment. *Cancer Res* **73**, 2480-92 (2013).

15. Lolmede, K. et al. Inflammatory and alternatively activated human macrophages

attract vessel-associated stem cells, relying on separate HMGB1- and MMP-9-dependent pathways. *J Leukoc Biol* **85**, 779-87 (2009).

16. Bao, S. et al. Stem cell-like glioma cells promote tumor angiogenesis through vascular endothelial growth factor. *Cancer Res* **66**, 7843-8 (2006).

17. Piao, Y. et al. Glioblastoma resistance to anti-VEGF therapy is associated with myeloid cell infiltration, stem cell accumulation, and a mesenchymal phenotype. *Neuro Oncol* **14**, 1379-92 (2012).

18. Prinz, M. & Priller, J. Microglia and brain macrophages in the molecular age: from origin to neuropsychiatric disease. *Nat Rev Neurosci* **15**, 300-12 (2014).

19. Wu, A. et al. Glioma cancer stem cells induce immunosuppressive macrophages/microglia. *Neuro Oncol* **12**, 1113-25 (2010).

20. Yang, J. et al. Tumor-associated macrophages regulate murine breast cancer stem cells through a novel paracrine EGFR/Stat3/Sox-2 signaling pathway. *Stem Cells* **31**, 248-58 (2013).

21. Watters, J.J., Schartner, J.M. & Badie, B. Microglia function in brain tumors. *J Neurosci Res* **81**, 447-55 (2005).

22. Guryanova, O.A. et al. Nonreceptor tyrosine kinase BMX maintains self-renewal and tumorigenic potential of glioblastoma stem cells by activating STAT3. *Cancer Cell* **19**, 498-511 (2011).

23. Nilsson, C.L. et al. Quantitative phosphoproteomic analysis of the STAT3/IL-6/HIF1alpha signaling network: an initial study in GSC11 glioblastoma stem cells. *J Proteome Res* **9**, 430-43 (2010).

24. Wang, H. et al. Targeting interleukin 6 signaling suppresses glioma stem cell survival and tumor growth. *Stem Cells* **27**, 2393-404 (2009).

25. Brat, D.J., Bellail, A.C. & Van Meir, E.G. The role of interleukin-8 and its receptors in gliomagenesis and tumoral angiogenesis. *Neuro Oncol* **7**, 122-33 (2005).

26. Letterio, J.J. & Roberts, A.B. Regulation of immune responses by TGF-beta. *Annu Rev Immunol* **16**, 137-61 (1998).

27. Gao, L. et al. Inhibition of STAT3 and ErbB2 suppresses tumor growth, enhances radiosensitivity, and induces mitochondria-dependent apoptosis in glioma cells. *Int J Radiat Oncol Biol Phys* **77**, 1223-31 (2010).

28. Liu, Y., Li, C. & Lin, J. STAT3 as a Therapeutic Target for Glioblastoma. *Anticancer Agents Med Chem* **10**, 512-9 (2010).

29. Markovic, D.S., Glass, R., Synowitz, M., Rooijen, N. & Kettenmann, H. Microglia stimulate the invasiveness of glioma cells by increasing the activity of metalloprotease-2. *J Neuropathol Exp Neurol* **64**, 754-62 (2005).

30. Nolte, C., Kirchhoff, F. & Kettenmann, H. Epidermal growth factor is a motility factor for microglial cells in vitro: evidence for EGF receptor expression. *Eur J Neurosci* **9**, 1690-8 (1997).

31. Meister, G. & Tuschl, T. Mechanisms of gene silencing by double-stranded RNA. *Nature* **431**, 343-9 (2004).

32. Wang, J. et al. siRNA targeting Notch-1 decreases glioma stem cell proliferation and tumor growth. *Mol Biol Rep* **39**, 2497-503 (2012).

33. Podesta, J.E. & Kostarelos, K. Chapter 17 - Engineering cationic liposome siRNA complexes for in vitro and in vivo delivery. *Methods Enzymol* **464**, 343-54 (2009).

34. Thurston, G. et al. Cationic liposomes target angiogenic endothelial cells in tumors and chronic inflammation in mice. *J Clin Invest* **101**, 1401-13 (1998).

35. Zhang, S., Zhao, B., Jiang, H., Wang, B. & Ma, B. Cationic lipids and polymers mediated vectors for delivery of siRNA. *J Control Release* **123**, 1-10 (2007).

36. Buyens, K. et al. Liposome based systems for systemic siRNA delivery: stability in blood sets the requirements for optimal carrier design. *J Control Release* **158**, 362-70 (2012).

37. Endoh, T. & Ohtsuki, T. Cellular siRNA delivery using cell-penetrating peptides modified for endosomal escape. *Adv Drug Deliv Rev* **61**, 704-9 (2009).

38. Ezzat, K. et al. Solid formulation of cell-penetrating peptide nanocomplexes with siRNA and their stability in simulated gastric conditions. *J Control Release* **162**, 1-8 (2012).

39. Jeong, J.H., Mok, H., Oh, Y.K. & Park, T.G. siRNA conjugate delivery systems. *Bioconjug Chem* **20**, 5-14 (2009).

40. Zhang, Y., Bradshaw-Pierce, E.L., Delille, A., Gustafson, D.L. & Anchordoquy, T.J. In vivo comparative study of lipid/DNA complexes with different in vitro serum stability: effects on biodistribution and tumor accumulation. *J Pharm Sci* **97**, 237-50 (2008).

41. Heddleston, J.M. et al. Hypoxia-induced mixed-lineage leukemia 1 regulates glioma stem cell tumorigenic potential. *Cell Death Differ* **19**, 428-39 (2012).

42. Garvalov, B.K. & Acker, T. Cancer stem cells: a new framework for the design of tumor therapies. *J Mol Med (Berl)* **89**, 95-107 (2011).

43. Eubank, T.D., Roda, J.M., Liu, H., O'Neil, T. & Marsh, C.B. Opposing roles for HIF-1alpha and HIF-2alpha in the regulation of angiogenesis by mononuclear phagocytes. *Blood* **117**, 323-32 (2011).

44. Komohara, Y. et al. Importance of direct macrophage-tumor cell interaction on progression of human glioma. *Cancer Sci* **103**, 2165-72 (2012).

45. Gedye, C. & Ailles, L. Isolation and characterization of cancer stem cells in vitro. *Methods Mol Biol* **946**, 181-204 (2013).

46. Yu, S.C. et al. Isolation and characterization of cancer stem cells from a human glioblastoma cell line U87. *Cancer Lett* **265**, 124-34 (2008).

47. Visnyei, K. et al. A molecular screening approach to identify and characterize inhibitors of glioblastoma stem cells. *Mol Cancer Ther* **10**, 1818-28 (2011).

48. Laks, D.R. et al. Neurosphere formation is an independent predictor of clinical outcome in malignant glioma. *Stem Cells* **27**, 980-7 (2009).

49. Bao, S. et al. Glioma stem cells promote radioresistance by preferential activation of the DNA damage response. *Nature* **444**, 756-60 (2006).

50. Wei, J. et al. Glioma-associated cancer-initiating cells induce immunosuppression. *Clin Cancer Res* **16**, 461-73 (2010).

51. Benayoun, L. & Shaked, Y. In vitro enrichment of tumor-initiating cells from human established cell lines. *Curr Protoc Stem Cell Biol* **Chapter 3**, Unit 3 7 (2013).

52. Panosyan, E.H. et al. Clinical outcome in pediatric glial and embryonal brain tumors correlates with in vitro multi-passageable neurosphere formation. *Pediatr Blood Cancer* **55**, 644-51 (2010).

53. Ye, X.Z. et al. Tumor-associated microglia/macrophages enhance the invasion of glioma stem-like cells via TGF-beta1 signaling pathway. *J Immunol* **189**, 444-53 (2012).

54. Creusat, G. et al. Proton sponge trick for pH-sensitive disassembly of polyethylenimine-based siRNA delivery systems. *Bioconjug Chem* **21**, 994-1002 (2010).

55. Huang, W., Lv, M. & Gao, Z. Polyethylenimine grafted with diblock copolymers of polyethylene glycol and polycaprolactone as siRNA delivery vector. *J Control Release* **152 Suppl 1**, e143-5 (2011).

56. Gao, Y., Liu, X.L. & Li, X.R. Research progress on siRNA delivery with nonviral carriers. *Int J Nanomedicine* **6**, 1017-25 (2011).

57. Harmon, A.M., Lash, M.H., Sparks, S.M. & Uhrich, K.E. Preferential cellular uptake of amphiphilic macromolecule-lipid complexes with enhanced stability and biocompatibility. *J Control Release* **153**, 233-9 (2011).

58. Sparks, S.M. et al. Efficient intracellular siRNA delivery by ethyleneimine-modified amphiphilic macromolecules. *Macromol Biosci* **11**, 1192-200 (2011).

59. Zhang, Y. et al. DC-Chol/DOPE cationic liposomes: a comparative study of the influence factors on plasmid pDNA and siRNA gene delivery. *Int J Pharm* **390**, 198-207 (2010).

60. Martino, S. et al. Efficient siRNA delivery by the cationic liposome DOTAP in human hematopoietic stem cells differentiating into dendritic cells. *J Biomed Biotechnol* **2009**, 410260 (2009).

61. Convertine, A.J. et al. pH-responsive polymeric micelle carriers for siRNA drugs. *Biomacromolecules* **11**, 2904-11 (2010).

62. Nuhn, L. et al. Cationic nanohydrogel particles as potential siRNA carriers for cellular delivery. *ACS Nano* **6**, 2198-214 (2012).

63. Wang, X.L., Xu, R. & Lu, Z.R. A peptide-targeted delivery system with pH-sensitive amphiphilic cell membrane disruption for efficient receptor-mediated siRNA delivery. *J Control Release* **134**, 207-13 (2009).

64. El Ouahabi, A. et al. The role of endosome destabilizing activity in the gene transfer process mediated by cationic lipids. *FEBS Lett* **414**, 187-92 (1997).

65. Yang, S. & May, S. Release of cationic polymer-DNA complexes from the endosome: A theoretical investigation of the proton sponge hypothesis. *J Chem Phys* **129**, 185105 (2008).

66. Hattori, Y. & Maitani, Y. Low-molecular-weight polyethylenimine enhanced gene transfer by cationic cholesterol-based nanoparticle vector. *Biol Pharm Bull* **30**, 1773-8 (2007).

67. Johannessen, T.C. & Bjerkvig, R. Molecular mechanisms of temozolomide resistance in glioblastoma multiforme. *Expert Rev Anticancer Ther* **12**, 635-42 (2012).

68. Pietras, A., Johnsson, A.S. & Pahlman, S. The HIF-2alpha-driven pseudo-hypoxic phenotype in tumor aggressiveness, differentiation, and vascularization. *Curr Top Microbiol Immunol* **345**, 1-20 (2010).

69. Xu, J., Zhao, Q., Jin, Y. & Qiu, L. High loading of hydrophilic/hydrophobic doxorubicin into polyphosphazene polymersome for breast cancer therapy. *Nanomedicine* **10**, 349-58 (2014).

70. Loew, S., Schmidt, U., Unterberg, A. & Halatsch, M.E. The epidermal growth factor receptor as a therapeutic target in glioblastoma multiforme and other malignant neoplasms. *Anticancer Agents Med Chem* **9**, 703-15 (2009).

71. Minchinton, A.I. & Tannock, I.F. Drug penetration in solid tumours. *Nat Rev Cancer* **6**, 583-92 (2006).

72. Sapra, P. & Allen, T.M. Ligand-targeted liposomal anticancer drugs. *Prog Lipid Res* **42**, 439-62 (2003).

73. Park, Y.S. Tumor-directed targeting of liposomes. *Biosci Rep* **22**, 267-81 (2002).